A Prognostic Cloud Scheme for Operational NWP Models

QINGYUN ZHAO

General Sciences Corporation/National Centers for Environmental Prediction, Washington, D.C.

FREDERICK H. CARR

School of Meteorology, University of Oklahoma, Norman, Oklahoma

(Manuscript received 28 November 1995, in final form 4 December 1996)

ABSTRACT

An explicit cloud prediction model has been developed and incorporated into the Eta Model at the National Centers for Environmental Prediction. In this scheme, only one predictive variable, cloud mixing ratio, is added to the model's prognostic equations to represent both cloud liquid water and cloud ice. Precipitation is diagnostically calculated from cloud mixing ratio. Extensive tests have been performed. The statistical results show a significant improvement in the model precipitation forecasts. Diagnostic studies suggest that the inclusion of cloud ice is important in transferring water vapor to precipitation and in the enhancement of latent heat release; the latter subsequently affects the vertical motion field significantly.

1. Introduction

Quantitative precipitation forecasting has been one of the weakest aspects of numerical weather prediction (NWP) models. One reason for the slow progress in precipitation forecasts is the simple treatment of condensation and precipitation processes in most operational models. In recent years, many NWP models have now become quite sophisticated in their advanced treatment of, for example, boundary layer processes and radiation. Their calculation of precipitation processes (especially the large-scale precipitation), however, is not carried out to the same degree of refinement. In some NWP models, the effects of clouds on condensation and evaporation are completely ignored in the calculation of precipitation. Although some reasonable precipitation forecasts have been produced by the simple precipitation schemes, one may argue that the neglect of cloud water and cloud ice can lead to some significant errors in the model thermodynamic and hydrological fields since clouds are the primary link connecting moisture and precipitation in the hydrological cycle of the atmosphere. Furthermore, the exclusion of ice-phase clouds in a model can lead to underestimates of latent heat released above the freezing level and therefore weakens the feedback of condensation to the thermodynamic fields.

In recent years, more and more modelers have realized that clouds play an important role in the prediction of dynamical, radiative, and hydrological processes. Efforts have been made to include the presence of clouds in both NWP and general circulation models (GCMs). A prognostic approach that contains an explicit calculation of cloud water content involving the formation and evaporation of clouds and precipitation was first proposed by Sundqvist (1978) and Sundqvist et al. (1989) for large-scale models. Following this work, an increased number of GCMs and NWP models have included a prognostic equation for the mass of cloud water and/or ice to parameterize the cloud processes (Golding 1990; Smith 1990; Pudykiewicz et al. 1992; Tiedtke 1993). This method is computationally more expensive than simple diagnostic methods since at least one additional prognostic variable to represent cloud water is required (some mesoscale models have four to five additional prognostic equations). However, the advantage of this method is that it allows proper representation of the thermodynamic effects of subgrid-scale condensation (precipitating and nonprecipitating), as well as a more direct link between the radiative, dynamical, and hydrological processes in the model.

The objective of this paper is to present and evaluate the performance of a prognostic cloud scheme for the Eta Model at the National Centers for Environmental Prediction (NCEP).[1] In this scheme, cloud water and

Corresponding author address: Dr. Qingyun Zhao, National Centers for Environmental Prediction, 5200 Auth Road, WWB, Room 207, Camp Springs, MD 20746.
E-mail: wd20cl@sun8.wwb.noaa.gov

[1] This scheme became operational at NCEP in August 1995 for the mesoscale Eta Model and in October 1995 in the early Eta Model.

TABLE 1. Definition of symbols in Eqs. (1), (2), and (3).

Symbol	Meaning
$\mathbf{V}_3\cdot\boldsymbol{\nabla}_3$	Three-dimensional advection
$\mathbf{V}_h\cdot\boldsymbol{\nabla}_h$	Horizontal advection
p	Pressure
R_d	Gas constant for dry air
C_p	Specific heat of air at constant pressure
ω	Vertical velocity in pressure coordiante (Pa s^{-1})
Q_r	Heating rate by radiation (K s^{-1})
E_c, E_r	Evaporation rate of cloud and precipitation (s^{-1})
C_b, C_g	Convective and grid-scale condensation rate (s^{-1})
C_b'	Net convective condensation rate (s^{-1})
P	Precipitation production rate from clouds (s^{-1})
P_{sm}	Melting rate of snow (s^{-1})
L	Latent heat of condensation/deposition
L_f	Latent heat of freezing

cloud ice are prognostically calculated in both stratiform and convective precipitation parameterizations. Since we wish to improve the model's quantitative precipitation forecasts, the new scheme should be complex enough to include all the important processes associated with precipitation. However, the scheme should be simple enough to minimize additional computational expense. Therefore, only one additional predictive variable, cloud mixing ratio, is added to the model's prognostic equations to represent both cloud water and cloud ice.

An important component in this research is the quantitative verification of precipitation forecasts for a large number of forecasts. Several quantitative precipitation forecast scores developed at NCEP were used in the precipitation verifications. The model prediction of cloudiness, an important field to model radiation and precipitation calculations, was also verified using satellite observations. Owing to the large variability of model forecasts from case to case, the new scheme was tested during several ''parallel tests'' at NCEP (some were done in real time; some were simulated over a longer period of time) instead of just for a few case studies. Another critical aspect of this work is the physical understanding of changes in model forecast fields caused by the inclusion of cloud water and cloud ice. Thus some special experiments were performed to study *how* the cloud water and cloud ice affect the model precipitation forecasts.

A description of the proposed scheme is presented in section 2. Section 3 outlines the design and procedures for validating the new cloud scheme and gives an evaluation of the results from the parallel tests and from the special experiments. A summary of the research and further discussion of the results are presented in section 4.

2. Description of the precipitation scheme

The main feature of the new precipitation parameterization scheme is the inclusion of cloud water and cloud ice in both the convective and grid-scale precipitation parameterizations. Instead of using two separate variables, we use only one predictive variable, the cloud water/ice mixing ratio m, to represent both cloud water and cloud ice. This will reduce the model computational time and storage requirements. Other simplifications, based on the work of previous investigators and tests performed here, have also been made to increase the efficiency of the scheme.

After incorporation of the cloud scheme, the model predictive equations for temperature T, specific humidity q, and cloud water/ice mixing ratio m are

$$\frac{\partial q}{\partial t} = q_{\text{non}} + E_c + E_r - C_b - C_g \tag{1}$$

$$\frac{\partial T}{\partial t} = T_{\text{non}} + \frac{L}{C_p}C_b + \frac{L}{C_p}C_g - \frac{L}{C_p}E_c - \frac{L}{C_p}E_r - \frac{L_f}{C_p}P_{sm} \tag{2}$$

$$\frac{\partial m}{\partial t} = m_{\text{non}} + C_b' + C_g - P - E_c, \tag{3}$$

where

$$q_{\text{non}} = -\mathbf{V}_3\cdot\boldsymbol{\nabla}_3 q + \text{turbulent term}$$

$$T_{\text{non}} = -\mathbf{V}_3\cdot\boldsymbol{\nabla}_3 T + \frac{\kappa\omega T}{p} + Q_r + \text{turbulent term}$$

$$m_{\text{non}} = -\mathbf{V}_h\cdot\boldsymbol{\nabla}_h m$$

$$\kappa = \frac{R_d}{C_p}.$$

The definition of the symbols in the equations above are listed in Table 1. It has been shown by Zhao (1993) that the total water defined by (1) and (3) is conserved. In order to reduce computational time, the vertical advection of m in (3) is ignored based on the assumption that for large-scale models in which the vertical motion is relatively weak, there is an approximate balance between the small gravitational fall speed of cloud particles and the model's large-scale vertical motion (Sundqvist et al. 1989).

Figure 1 shows a schematic illustration of the precipitation scheme. There are two sources of condensation, one from large-scale processes and the other from convective processes. Both of them produce either cloud water or cloud ice, depending on the cloud substance at and above the grid point at current and previous time steps, and on the temperature. Evaporation of cloud is allowed at points where the relative humidity is lower than the critical value required for condensation. Precipitation is diagnostically calculated directly from the cloud water/ice mixing ratio. Both frozen and liquid precipitation can be prognostically produced, enabling this scheme to predict precipitation type.

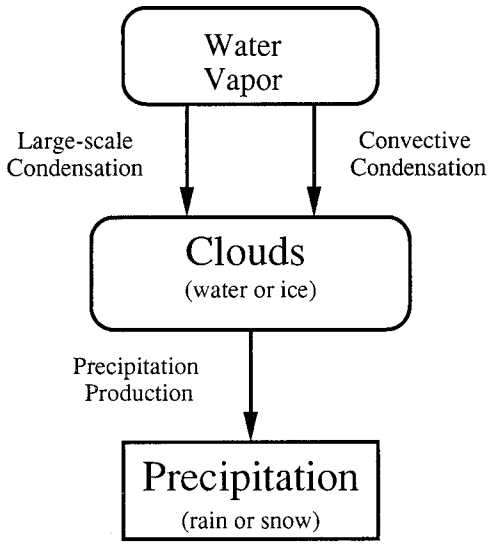

FIG. 1. Schematic illustration of the new precipitation scheme.

a. Large-scale condensation (C_g)

If we let

$$A_q = q_{\text{non}} + E_r - C_b \tag{4}$$

$$A_t = T_{\text{non}} + \frac{L}{C_p}C_b - \frac{L}{C_p}E_r - \frac{L_f}{C_p}P_{sm}, \tag{5}$$

then (1) and (2) become

$$\frac{\partial q}{\partial t} = A_q + E_c - C_g \tag{6}$$

$$\frac{\partial T}{\partial t} = A_t - \frac{L}{C_p}E_c + \frac{L}{C_p}C_g. \tag{7}$$

Following Sundqvist (1988), an expression for large-scale condensation rate C_g can be obtained by combining (6) and (7) with equations $q = fq_s$, $q_s = \epsilon e_s/p$, and the Clausius–Clapeyron equation $de_s/dT = \epsilon L e_s/RT^2$, where q_s is the saturation specific humidity, e_s is the saturation vapor pressure, R is the specific gas constant for dry air, p is the pressure, f is the relative humidity, and $\epsilon = 0.622$. The expression for C_g has the form

$$C_g = \frac{M - q_s f_t}{1 + (f\epsilon L^2 q_s/RC_p T^2)} + E_c, \tag{8}$$

where

$$M = A_q - \frac{f\epsilon L q_s}{RT^2}A_t + \frac{fq_s\partial p}{p\partial t}. \tag{9}$$

To close the system, an equation for relative humidity tendency f_t was derived by Sundqvist et al. (1989) using the hypothesis that the quantity $M + E_c$ is divided into one part, bM, which condenses in the already cloudy portion of a grid square, and another part, $(1 - b)M + E_c$, which is used to increase the relative humidity of the cloud-free portion and to increase the cloudiness in the square. The equation is written as

$$f_t = \frac{2(1 - b)(f_s - f_0)[(1 - b)M + E_c]}{2q_s(1 - b)(f_s - f_0) + m/b}, \tag{10}$$

where $f_s = 1$, f_0 is the critical value of relative humidity for condensation and b is the cloud coverage calculated using the equation (Sundqvist et al. 1989)

$$b = 1 - \left(\frac{f_s - f}{f_s - f_0}\right)^{1/2}. \tag{11}$$

When $f < f_0$, $b = 0$. The parameter f_0 accounts for the effects of subgrid-scale variations in moisture on large-scale condensation. Its value is important to the calculation of condensation, evaporation, and precipitation. In our experiments, f_0 was empirically set to 0.75 over land and 0.90 over ocean based on sensitivity studies.

TABLE 2. The IW values in different temperature regions.

Temperature	Large-scale condensation	Convective condensation
$T > 0$°C	IW = 0	IW = 0
-15°C $< T < 0$°C	IW = 1, if there is cloud ice at or above this point at current or the previous time step;	
	IW = 0, otherwise.	IW = 1
$T < -15$°C	IW = 1	IW = 1

Since the scheme proposed here includes cloud ice, the relative humidity f should be calculated with respect to water in cloud water regions and with respect to ice in cloud ice regions. Therefore, we need to know where cloud ice exists. The distinction between cloud water and cloud ice is made by the cloud identification number IW, which is zero for cloud water and unity for cloud ice. The determination of IW at one point is based on the temperature at this point at the current time step and the cloud substance at and above this point at the current and one previous time step. Table 2 shows the values of IW in different temperature regions. All clouds are defined to consist of liquid water below the freezing level and of ice particles above the $T = -15$°C level. In the temperature region between these two, clouds may be either cloud water or cloud ice. If there are cloud ice particles above this point at the previous or current time step, or if the cloud at this point at the previous time step consists of ice particles, then the cloud substance at this point should also be ice particles because of the cloud seeding effect and the cloud memory of its content. Otherwise, all clouds in this region are considered to contain supercooled cloud water.

b. Convective condensation (C_b, C_b')

A modified version of the Betts–Miller convective parameterization scheme (Betts 1986; Betts and Miller

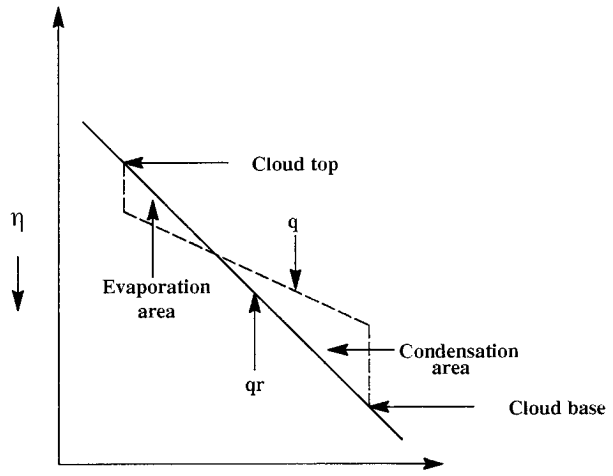

FIG. 2. Schematic representation of condensation and evaporation in the Betts–Miller convective adjustment scheme. (q—model's profile of specific humidity; q_r—reference profile.)

1986) has been adapted to account for the inclusion of cloud water and cloud ice as a prognostic variable. Reference profiles of temperature T_r and moisture q_r have been constructed based on numerous observations. The model profiles of T and q at points where deep convection occurs are adjusted toward the reference profiles. The total enthalpy, $H = C_pT + Lq$, will be conserved during the adjustment process, that is,

$$\int_{\eta_t}^{\eta_b} (H_r - H)\, d\eta = 0, \tag{12}$$

where H_r is the reference profile of enthalpy, η is the vertical coordinate of the model, and η_t and η_b are the model levels at cloud top and cloud base, respectively. The moisture change at a grid point due to the moisture adjustment is parameterized by

$$C_b = \frac{q - q_r}{\tau}, \tag{13}$$

where τ is the timescale of convective adjustment. The condensation rate C_b must be modified to produce the three-dimensional convective cloud required in our scheme. Figure 2 gives a schematic representation of the moisture adjustment process. Consider an atmospheric column where deep convection occurs. At some levels $q > q_r$ and $C_b > 0$ (condensation), while at others, $q < q_r$ and $C_b < 0$ (evaporation). Therefore, some of the condensed water produced at condensation points must be transferred to the points where $C_b < 0$ and evaporated in order to complete the convective adjustment process. It is assumed that vertical mixing inside the convective clouds is strong enough that some of the cloud water formed at condensation points is immediately transferred to the evaporation points for evaporation. The rest of the cloud water is assumed to stay at the condensation points, and therefore the final net condensation rate C_b' at each level is calculated from

$$C_b' = RB, \tag{14}$$

where the ratio R is calculated from

$$R = \frac{\int_{\eta_t}^{\eta_b} C_b\, d\eta}{\int_{\eta_t}^{\eta_b} B\, d\eta} \qquad (R \le 1), \tag{15}$$

and $B = C_b$ if $C_b \ge 0$ and $B = 0$ if $C_b < 0$. The constraint for C_b' is

$$\int_{\eta_t}^{\eta_b} C_b'\, d\eta = \int_{\eta_t}^{\eta_b} C_b\, d\eta. \tag{16}$$

If $\int_{\eta_t}^{\eta_b} C_b\, d\eta < 0$, no adjustment is allowed (Janjić 1994). The net convective condensation rate C_b' is used to calculate cloud production at convective points. The determination of IW values for convection is given in Table 2. In the temperature region between 0° and −15°C, IW is set to 1 since most convective clouds have cloud tops above the $T = -15$°C level.

The difference between the original Betts–Miller scheme and this scheme is that the modified scheme does not produce convective precipitation by itself. Instead, it produces convective clouds at convective points that are then merged with the clouds from large-scale condensation. Total precipitation (both large-scale and convective) is then calculated from the clouds through the microphysical processes given in section 2d. This allows the influence of microphysics on the production of convective precipitation. The determination of cloud coverage b at convective points remains a difficult problem in this scheme. Since the cloud cover influences precipitation production only via the process of autoconversion of cloud water to rain [see (24)], our experiments showed that the impact of convective cloud cover on precipitation is relatively weak. For simplicity, we set b to a constant between zero and unity. Experiments showed that $b = 0.5$ gave the best precipitation forecast results.

c. Cloud evaporation (E_c)

Cloud evaporation is allowed to take place only where the relative humidity $f < f_0$, that is, where there is no condensation occurring at this point. Sometimes cloud evaporation can be stopped by the saturation caused by the moisture increase from the cloud evaporation before all clouds have been evaporated. To ensure that the relative humidity f does not exceed the critical value f_0 during cloud evaporation, our scheme assumes that only part of the cloud evaporates and all water vapor from evaporation is used to increase the relative humidity f until f_0 is reached. If q_0 represents the specific humidity at relative humidity f_0, then

$$q_0 = f_0 q_s. \tag{17}$$

In the case where the cloud water/ice at this point is enough to be evaporated until f_0 is reached, then the evaporation rate E_c, if we assume that the evaporation process occurs in one time step, is determined by

$$E_c = \frac{q_0 - q}{\Delta t}. \tag{18}$$

Using (17) and the equation $q = fq_s$, E_c then becomes

$$E_c = \frac{q_s}{\Delta t}(f_0 - f), \tag{19}$$

where Δt is the time step for precipitation calculation in the model. In the case where all clouds will evaporate before f_0 is reached, the following equation is used:

$$E_c = \frac{m}{\Delta t}. \tag{20}$$

Equation (19) is a simplified version of a higher-order cloud evaporation algorithm (Rutledge and Hobbs 1983). Results from the experiments designed to test (19) and (20) (not shown) revealed that very small differences were found in forecasts between the simplified and the higher-order methods, indicating that the simplified method can be used with this cloud scheme.

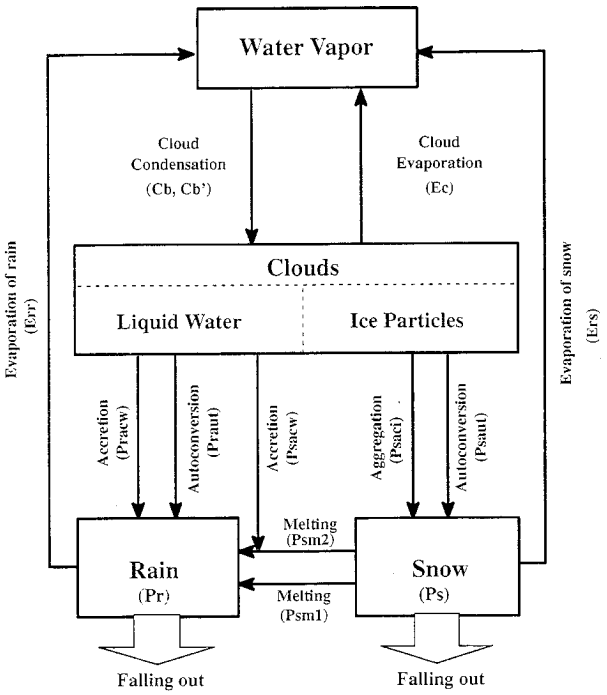

FIG. 3. Microphysical processes simulated in the new precipitation scheme.

d. Precipitation production (P, P_{sm} E_r)

Precipitation is the last step of the atmospheric hydrological cycle. The parameterization of precipitation production is required in order to remove water substance from the atmosphere to the ground. The difficulties in the precipitation production calculation arise from the complexity of the precipitation formation process that involves complicated interactions among precipitation particles of different sizes, shapes, and phases. A complete description of precipitation formation requires a good understanding of the characteristics and behavior of the different hydrometers in the atmosphere.

In the scheme discussed here, however, simplifications in the precipitation parameterization are needed due to the limitations in computational time and computer storage required by operational NWP models. First, consideration of particle size and shape can be avoided by using the bulk parameterization method introduced by Kessler (1969). Second, only two types of precipitation, rain and snow, are considered in this scheme. Third, only the principle microphysical processes associated with the formation of rain and snow are included. Figure 3 presents the microphysical processes considered in the precipitation parameterization. Basically, there are four types of microphysical processes considered here: production of rain from cloud water, production of snow from cloud ice, melting of snow to form rain below the freezing level, and the evaporation of precipitation. Some processes, such as the freezing of raindrops and the interaction between rain drops and cloud ice, have been ignored since the upward motion on the synoptic scale is too weak to advect the raindrops upward. Finally, the fourth simplification is that precipitation is diagnostically calculated directly from the cloud mixing ratio. This eliminates the computation of the terminal velocities of precipitation particles that requires much computer time. More importantly, a number of predictive equations for different types of precipitation that would normally be needed by the model have been avoided by this simplification.

From Fig. 3, the precipitation terms in (1)–(3) can be represented by

$$P = P_{\text{raut}} + P_{\text{saut}} + P_{\text{racw}} + P_{\text{sacw}} + P_{\text{saci}} \tag{21}$$

$$P_{sm} = P_{sm1} + P_{sm2} \tag{22}$$

$$E_r = E_{rr} + E_{rs}. \tag{23}$$

Following Sundqvist et al. (1989), the autoconversion of cloud water to rain, P_{raut}, can be parameterized from the cloud water mixing ratio m and cloud coverage b, that is,

$$P_{\text{raut}} = c_0 m\left\{1 - \exp\left[-\left(\frac{m}{m_r b}\right)^2\right]\right\}, \tag{24}$$

where constants c_0 and m_r are 1.0×10^{-4} s^{-1} and 3.0×10^{-4}, respectively. The autoconversion of cloud ice to snow is simulated using the equation from Lin et al. (1983)

$$P_{\text{saut}} = a_1(m - m_{i0}), \tag{25}$$

where m_{i0} is the threshold of cloud ice mixing ratio for production of snow from cloud ice and is set to a value of 1.0×10^{-4} (kg kg^{-1}). Since snow production in this process is caused by the size increases of cloud ice particles due to depositional growth and aggregation among small ice particles, P_{saut} should be a function of temperature. According to Lin et al. (1983), a_1 is specified as a function of temperature to account for the temperature effects on P_{saut} and is given by

$$a_1 = 10^{-3} \exp[0.025(T - 273.15)]. \quad (26)$$

The collection of cloud substance by falling precipitation is another important process that converts cloud water/ice to precipitation. In the regions where cloud water and rain exist, the accretion of cloud water by rain, P_{racw}, can be expressed using the cloud mixing ratio m and rainfall rate P_r, that is,

$$P_{\text{racw}} = C_r m P_r, \quad (27)$$

where C_r is the collection coefficient. From our experiment results, $C_r = 5.0 \times 10^{-4}$ m^2 kg^{-1} s^{-1} gives a reasonable value of P_{racw}. Another aggregation process is the collection of cloud ice by snow in the regions where cloud ice exists. Similarly, we can simulate this process by

$$P_{\text{saci}} = C_s m P_s, \quad (28)$$

where P_s is the precipitation rate of snow. The difference between (27) and (28) is that the collection coefficient C_s should be a function of temperature since the open structures of ice crystals at relative warm temperatures are more likely to stick, given a collision, than crystals of other shapes (Rogers 1979). Above the freezing level, C_s is expressed by

$$C_s = c_1 \exp[c_2(T - 273.15)] \quad (29)$$

and zero below. In our experiments, $c_1 = 1.25 \times 10^{-3}$ m^2 kg^{-1} s^{-1} and $c_2 = 0.025$ K^{-1} are used.

The treatment of the melting layer is important to both precipitation and dynamic calculations in the regions around the melting layer. First, melting of snow below the freezing level converts ice-phased precipitation to liquid water. Second, the latent heat release due to the water phase change will affect the thermodynamic and dynamic fields in this region. In this scheme, we allow the melting of snow to take place in certain temperature regions below the freezing level in two ways. One is the continuous melting of snow due to the increase in temperature as it falls down through the freezing level. Another is the immediate melting of melting snow by collection of the cloud water below the freezing level. The melted snow in both cases is assumed to become raindrops. The first melting process can be parameterized as a function of temperature and snow precipitation rate, that is,

$$P_{sm1} = C_{sm} (T - 273.15)^{\alpha} P_s. \quad (30)$$

From our experiments, parameter values of $C_{sm} = 5 \times 10^{-8}$ m^2 kg^{-1} K^{-2} s^{-1} and $\alpha = 2$ cause the falling snow to melt almost completely before it reaches the $T = 278.15$ K level.

The second melting process, that is, the interaction between melting snow and cloud water below the freezing level, is different from the first melting process. First, the heat needed to melt the melting snow comes from the cloud water at the surrounding atmosphere temperature. Therefore, the melting rate of snow in this process depends on how much cloud water the snow has collected. Second, both cloud water and melting snow are converted to rain during this process. In order to calculate the melting rate, we need to compute the collection rate of cloud water by melting snow first. Similar to the collection of cloud water by rain, the collection of cloud water by melting snow can be parameterized to be proportional to the cloud water mixing ratio m and the precipitation rate of snow P_s, that is,

$$P_{\text{sacw}} = C_r m P_s, \quad (31)$$

where C_r is the collection coefficient in (27). The melting rate of snow then can be computed from

$$P_{sm2} = C_{ws} P_{\text{sacw}}. \quad (32)$$

To determine the parameter C_{ws}, we need to assume that the temperature of collected droplets ranges from 0° to 4°C (about 500 m below the freezing level) and that the melting snow has a temperature of 0°C. Therefore, the average temperature difference between the melting snow and the collected droplets $\Delta T \approx 2$°C. The heat balance equation then can be written as

$$C_w m_w \Delta T = L_f m_s, \quad (33)$$

where C_w is the specific heat of water, L_f is the latent heat of melting, m_w is the mass of collected cloud water, and m_s is the mass of collecting snow. From (32),

$$C_{ws} = \frac{P_{sm2}}{P_{\text{sacw}}} = \frac{m_s}{m_w} = \frac{C_w \Delta T}{L_f} \approx 0.025. \quad (34)$$

The evaporation of precipitation is important in moistening the layers below cloud base. Through this process, some of the precipitating water is evaporated back to the atmosphere and the precipitation efficiency is reduced. Unlike the precipitation evaporation scheme in the original operational Eta Model (80-km version) at NCEP in which precipitation cannot fall to the ground until the whole subcloud layer is saturated (Janjić 1990), some precipitation in this scheme can still fall through the unsaturated subcloud layer while it is evaporating (as it does in the real atmosphere). Evaporation of rain is allowed in this scheme at points where relative humidity $f < f_0$ and is calculated using the equation (Sundqvist 1988)

$$E_{rr} = k_e (f_0 - f)(P_r)^{\beta}, \quad (35)$$

where k_e and β are parameters that need to be determined empirically. In our experiments, $k_e = 2 \times 10^{-5}$ m^1 kg$^{-0.5}$ s^{-1} and $\beta = 0.5$ gave reasonable values of rain evap-

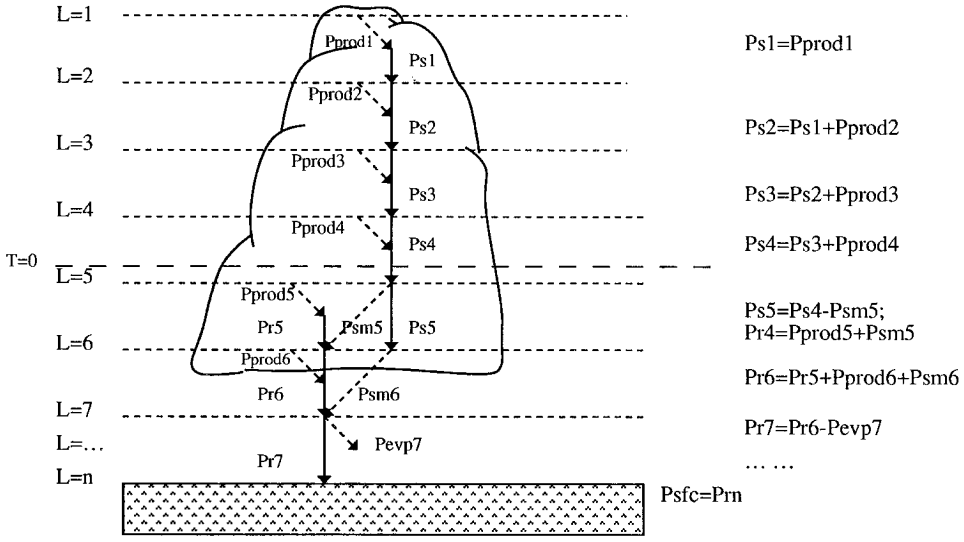

FIG. 4. The procedure for precipitation computation in the new precipitation scheme. (P_{prodi}—production of precipitation from cloud water/ice at the ith level; P_{si}—precipitation of snow from the ith level; P_{ri}—precipitation of rain from the ith level; P_{evpi}—evaporation of precipitation at the ith level; P_{smi}—melting of snow at the ith level; P_{sfc}—precipitation on the surface; n—the model level above the surface.)

oration. The evaporation of snow at points with relative humidity $f < f_0$ is calculated using the equation

$$E_{rs} = [(C_{rs1} + C_{rs2}(T - 273.15)]\left(\frac{f_0 - f}{f_0}\right)P_s, \quad (36)$$

where $C_{rs1} = 5 \times 10^{-6}$ m^2 kg^{-1} s^{-1} and $C_{rs2} = 6.67 \times 10^{-10}$ m^2 kg^{-1} K^{-1} s^{-1}. The evaporation of melting snow below the freezing level is ignored in this scheme because of the difficulty in the latent heat treatment since the surface of a melting snowflake is usually covered by a thin layer of liquid water.

e. Implementation of the scheme

So far we have derived the equations necessary to calculate all the terms associated with phase changes of water substance on the right-hand sides of (1)–(3). The quantities we need to close this system are the precipitation rates of rain and snow at each model level. The following two equations can be used to calculate them:

$$P_r(\eta) = \frac{p_s - p_t}{g\eta_s}\int_{\eta}^{\eta_t}(P_{\text{raut}} + P_{\text{racw}} + P_{\text{sacw}} + P_{sm1} + P_{sm2} - E_{rr})\,d\eta \quad (37)$$

and

$$P_s(\eta) = \frac{p_s - p_t}{g\eta_s}\int_{\eta}^{\eta_t}(P_{\text{saut}} + P_{\text{saci}} - P_{sm1} - P_{sm2} - E_{rs})\,d\eta, \quad (38)$$

where p_s and p_t are the surface pressure and the pressure at the top of model domain, respectively, and g is gravity. The expression for η_s is defined by (Mesinger et al. 1988)

$$\eta_s = \frac{p_{\text{ref}}(z_{\text{sfc}}) - p_t}{p_{\text{ref}}(0) - p_t}, \quad (39)$$

where p_{ref} (z_{sfc}) and p_{ref} (0) are the reference pressures on surfaces with height z_{sfc} and sea level, respectively.

The difficulty in computing P_r and P_s is that some terms on the right-hand sides of (37) and (38) are functions of P_r and P_s. For simplicity, an explicit computational procedure has been designed to solve this problem. An example of the procedure is given in Fig. 4, where we assume that the cloud top here is high enough so that the cloud above the freezing level consists of ice particles. At each η level, the precipitation production terms on the right-hand sides of (37) and (38) are computed first using the precipitation rate of rain (and/or snow) from the level above. Then all precipitation production at this level is added to the precipitation from the level above to give the precipitation rate for the next level calculation. This procedure is done level by level, downward from cloud top. Note that rain and melting snow can coexist in the region below the freezing level and collisions between these two types of precipitation have been ignored. The total precipitation at the surface can be calculated from

$$P_{\text{sfc}} = \frac{P_r(\eta_{\text{sfc}}) + P_s(\eta_{\text{sfc}})}{\rho_w}, \quad (40)$$

where η_{sfc} is the η level at the surface and ρ_w the liquid water density. The units of P_{sfc} are in meters. If the surface temperature is low enough, snow or melting snow can accumulate on the surface. Thus, this scheme is able to predict precipitation type.

TABLE 3. Summary of parallel tests for evaluation of the precipitation scheme.

Parallel tests	I	II	III	IV
Periods	December 1990 to April 1991	9 August to 24 August 1991	31 December 1991 to 31 January 1992	14 April to 4 May 1992
Major precipitation type	Winter and spring tratiform precipitation; toward the end, there was convective activity	Summer strong convections	Winter stratiform precipitation	Mixture of stratiform and convective precipitation during the spring and early summer
Number of cases	27	16	31	21
Case selection	Whenever significant precipitation over U.S.	Each day	Each day except 12 January (data missing)	Each day
Daily times of forecasts	One 48-h forecast started at 1200 UTC of each selected day	Two 48-h forecasts started at 0000 and 1200 UTC of each day	One 48-h forecast started at 1200 UTC of each day	Two 48-h forecasts started at 0000 and 1200 UTC of each day
Eta Model resolution	80 km × 16 levels	80 km × 16 levels	80 km × 16 levels	80 km × 17 levels

3. Precipitation forecast comparisons

a. Description of the Eta Model

Tests of the proposed prognostic cloud scheme were performed with a modified research version of the step-mountain, eta-coordinate regional numerical weather prediction model (Eta Model) operational at NCEP from 1993 to 1995. The Eta Model was chosen for our precipitation scheme tests for two reasons. First, this model is the newest model developed for regional operational forecasts at NCEP. Advanced numerical techniques and physical parameterization methods have been incorporated into the model (Mesinger et al. 1988; Janjić 1990, 1994). Second, one of the main purposes for developing the Eta Model at NCEP is to improve precipitation forecasts over North America. As indicated by Black and Mesinger (1989) and Black et al. (1990), precipitation forecasts from the Eta Model have

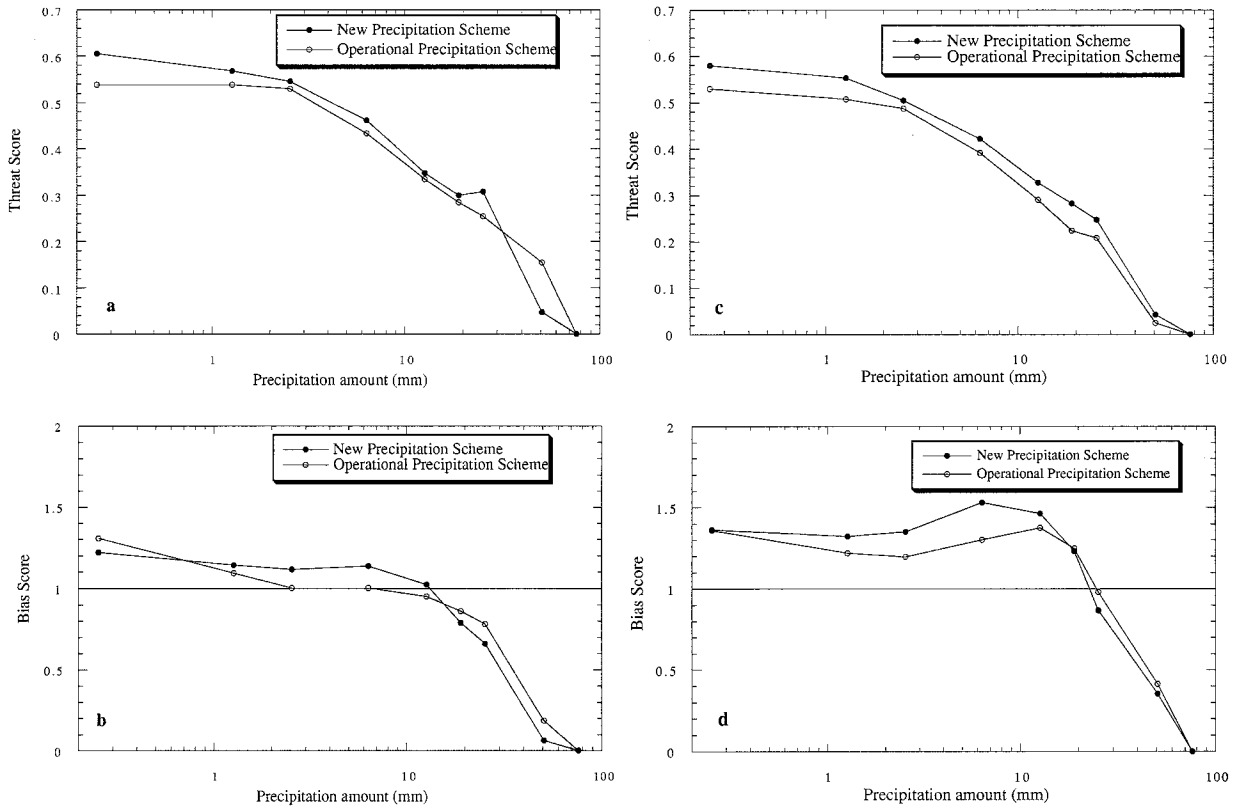

FIG. 5. The threat and bias scores averaged over 27 cases of precipitation forecasts from the operational runs and the experiments using the new precipitation scheme during test I: (a), (b) 0–24-h forecasts; (c), (d) 24–48-h forecasts.

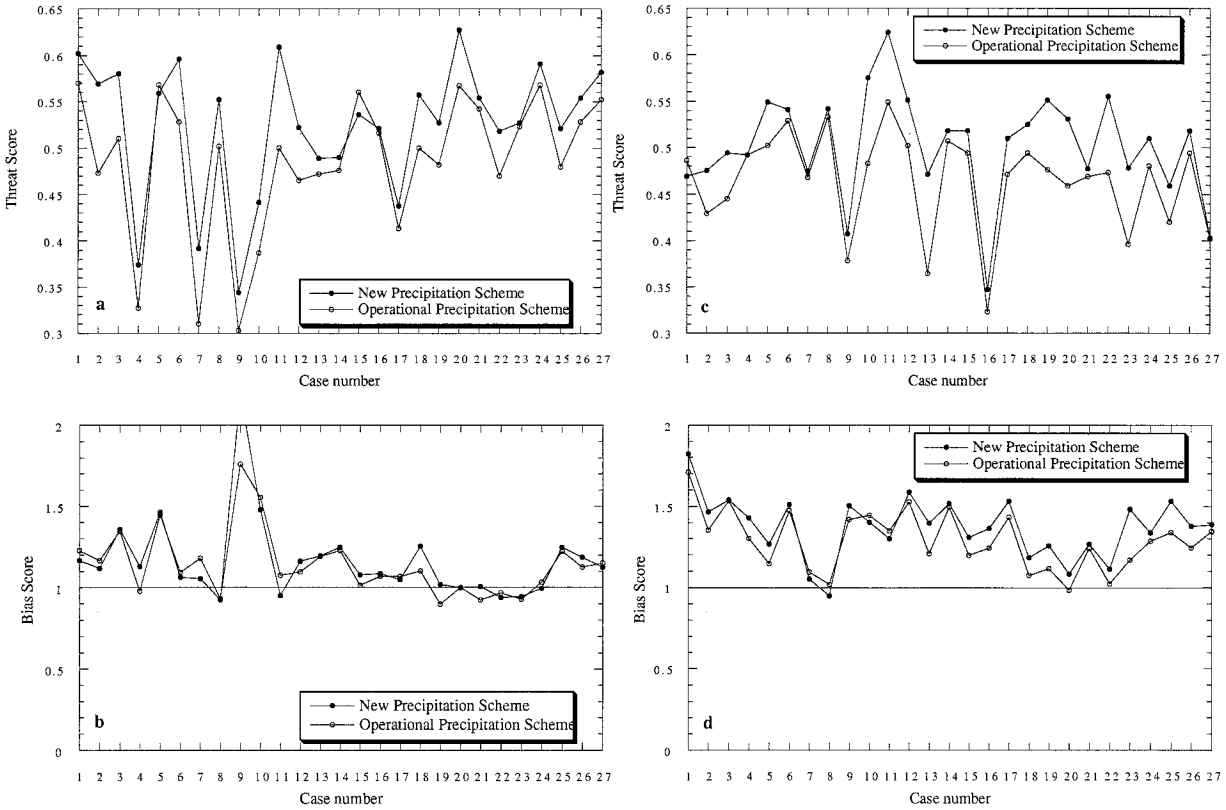

FIG. 6. The threat and bias scores from operational and experimental runs averaged over precipitation thresholds for all events in case I: (a), (b) 0–24-h forecasts; (c), (d) 24–48-h forecasts.

been improved substantially over the Nested Grid Model, especially for high amounts. Thus, it will be a greater challenge to see if the proposed cloud scheme will improve already superior forecasts of precipitation. Examples of Eta Model performance are contained in Black and Mesinger (1989) and Black (1994). Here we will give a brief overview of the main features of the model.

The Eta Model was first developed by Mesinger et al. (1988). A comprehensive physical package has been incorporated into the model by Janjić (1990). The horizontal grid structure in the Eta Model is the semistaggered E grid. In the vertical direction, the eta coordinate proposed by Mesinger et al. (1988) is used to eliminate the computational errors in the sigma-coordinate pressure gradient terms over steep terrain. The model domain covers all of North America and parts of the Pacific and Atlantic Oceans. Time-dependent lateral boundary conditions are provided by the previous run of NCEP's global spectral model. The Janjić (1984) horizontal advection scheme is used in conjunction with a modified Euler-backward time scheme. The Euler-backward time and centered-space difference scheme is used for vertical advection for all quantities except specific humidity q, for which an upstream spatial differencing scheme is used. With the current code, the model can be run at any horizontal and vertical resolution. During our studies, the operational and our test models ran with 80-km horizontal resolution and 17 vertical levels.

The Mellor–Yamada second-order closure theory (Mellor and Yamada 1974, 1982) is used to describe the turbulent transfer processes. For parameterization of both shortwave and longwave radiation, the radiation package developed at the Geophysical Fluid Dynamics Laboratory (Lacis and Hansen 1974; Fels and Schwarzkopf 1975) is used. In the operational version, the method developed by Hoke et al. (1989) is used to calculate the large-scale condensation. This method sets a critical value of relative humidity. If model relative humidity is greater than the critical value, condensation occurs at this grid point. The condensation is summed layer by layer downward from the top. If a layer is subsaturated, the water is evaporated until the layer becomes saturated with respect to the critical value. The water reaching the ground becomes precipitation. Corresponding changes in temperature and specific humidity resulting from condensation and evaporation are calculated. A modified convective adjustment scheme originally proposed by Betts (1986) and Betts and Miller (1986) is used to determine model convective rainfall. This approach involves construction of reference profiles of temperature and specific humidity based on numerous observations and then relaxing the ambient profiles toward them if convective precipitation occurs. The con-

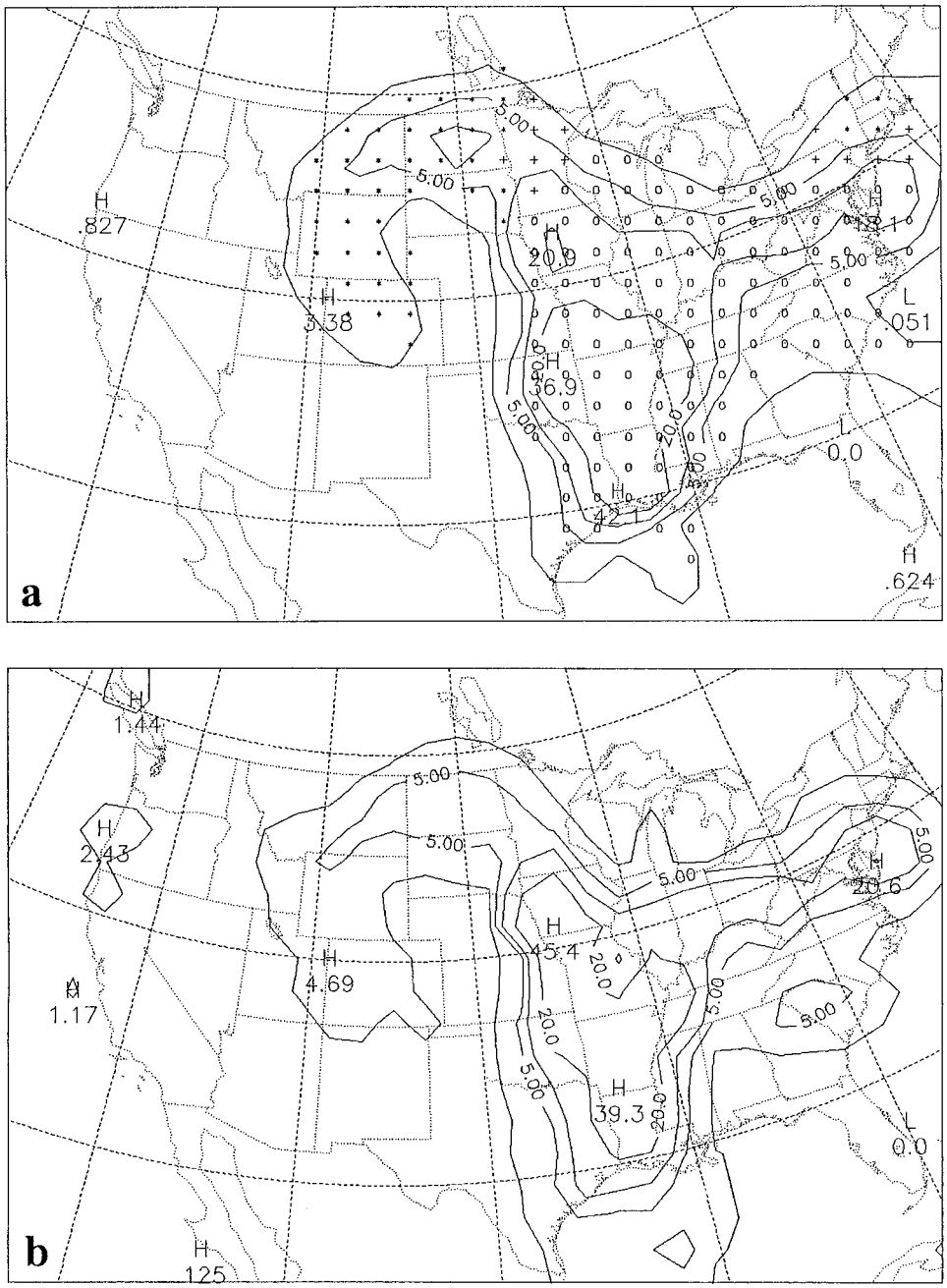

FIG. 7. Precipitation distributions for 1200 UTC 14 April 1991. (a) 24-h forecast from the new precipitation scheme; (b) 24-h forecast from the operational run; and (c) observed precipitation. Contours are 1, 5, 10, 20, and 50 mm. Asterisks represent snow, circles rain, and crosses both snow and rain.

vective precipitation is computed by vertically integrating the moisture adjustment over a grid box during the convective adjustment.

b. Verification procedures

As mentioned before, the accuracy of model precipitation forecasts can vary significantly from day to day and from season to season due to the sensitivity of the model initial conditions, dynamics, and physical parameterizations to the variations in weather situations. Statistical evaluation of the precipitation forecasts over a long period of time should be used to eliminate these fluctuations in the accuracy of model precipitation forecasts and to get a more reliable measure of the precipitation scheme performance. Based on this consideration, several parallel tests were performed at NCEP during a 17-month period. Table 3 gives a summary of the

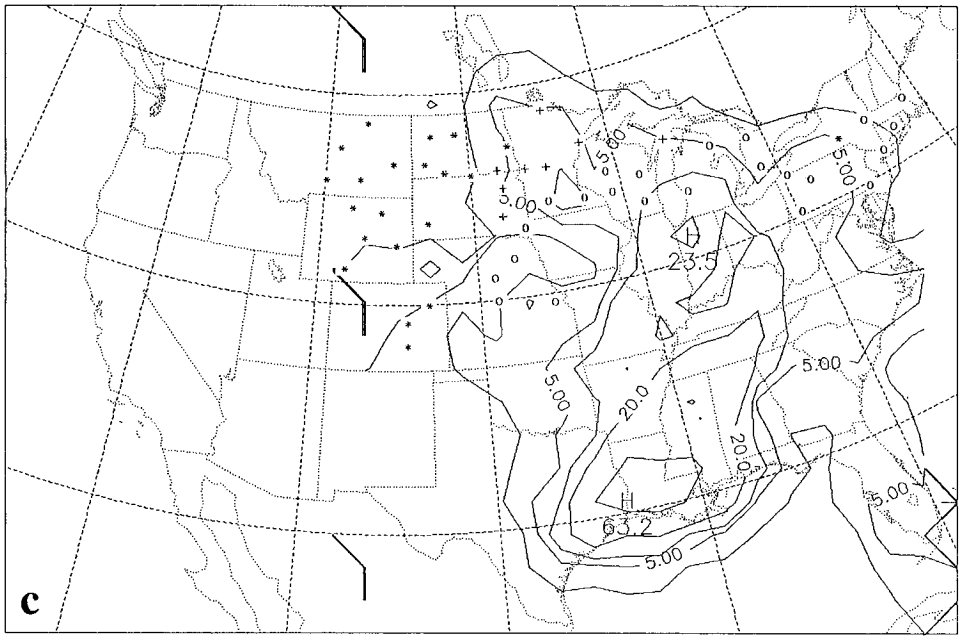

FIG. 7. (*Continued*)

parallel tests we have done. These tests were designed for different seasons with different types of precipitation. To limit the length of this discussion, we will present the results from two parallel tests that best represent the performance of the precipitation scheme.

The data analysis system at NCEP was used to obtain the initial fields and boundary conditions for our version of the Eta Model. The 24-h observed precipitation analyses operationally available at NCEP were used to verify the precipitation forecasts. The precipitation analysis combines reports of daily precipitation data provided by the River Forecast Centers and synoptic reports with manually digitized radar data from the WSR-57 radar network (Baldwin 1991). Since the precipitation analysis is valid at 1200 UTC of each day, a 48-h precipitation forecast can be verified twice (0–24-h forecast and 24–48-h forecast) if it is started at 1200 UTC and only once (12–36-h forecast) if it is started at 0000 UTC.

The objective evaluation of quantitative precipitation forecasts was performed by calculating forecast biases (BIAS), precipitation threat scores (THRT), equitable threat scores (EQTS), and equitable skill scores (EQSS) for various quantitative precipitation categories. The definitions of these scores are given in the appendix.

c. Experiment results

1) PRECIPITATION FORECAST IMPROVEMENT

We first show results from test period I, which Table 3 indicates covers a period in which we selected 27 days where significant precipitation occurred. Figure 5 shows the average threat scores and biases in each precipitation category for 24-h and 48-h forecasts, respectively, during test I. The averages for each precipitation threshold were calculated using the equations

$$\langle \mathrm{THRT} \rangle_i = \sum_{n=1}^{N} a_{i,n} (\mathrm{THRT})_{i,n} \tag{41}$$

$$\langle \mathrm{BIAS} \rangle_i = \sum_{n=1}^{N} a_{i,n} (\mathrm{BIAS})_{i,n}, \tag{42}$$

where i is the index of precipitation threshold, n is the case index, and N is the total number of cases during the test period. The weight function $a_{i,n}$ was calculated by

$$a_{i,n} = \frac{\begin{array}{c}(\text{grid number of observations}\\ \text{in each threshold for each case})\end{array}}{\begin{array}{c}(\text{grid number of observations}\\ \text{in each threshold for all cases}).\end{array}} \tag{43}$$

The averages weighted by the grid number of observations used here can eliminate the overweighting of scores from cases with a small number of observation grid points. It can be seen from Fig. 5 that the average threat scores improved significantly for all precipitation thresholds for both 24- and 48-h forecasts, except for the 50-mm precipitation amount in 24-h forecasts. The largest improvement is in the light precipitation region, indicating that the prognostic cloud scheme is better than the operational scheme in predicting the total precipitation area. The average bias scores from the new scheme are somewhat higher in the middle range of precipitation amounts than those from the operational model. The increases in biases mean that the forecast precipitation areas for the middle range have been enlarged. However, we have increased the skill of the 0.25-mm area without increasing the bias. Another way

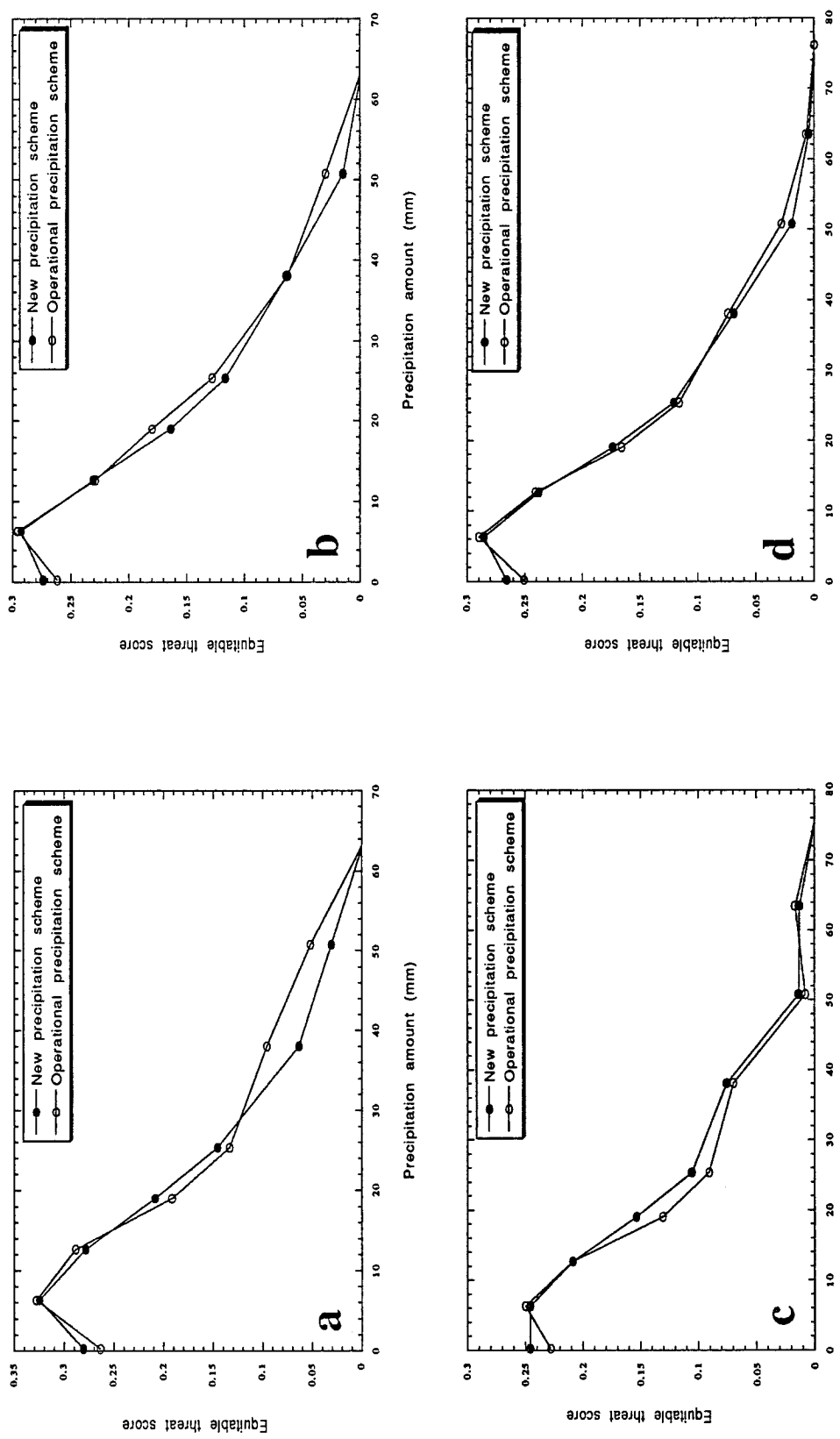

FIG. 8. Average equitable threat scores for precipitation forecasts from the operational and new precipitation schemes in test IV: (a) 0–24-h forecasts; (b) 12–36-h forecasts; (c) 24–48-h forecasts; (d) all forecasts.

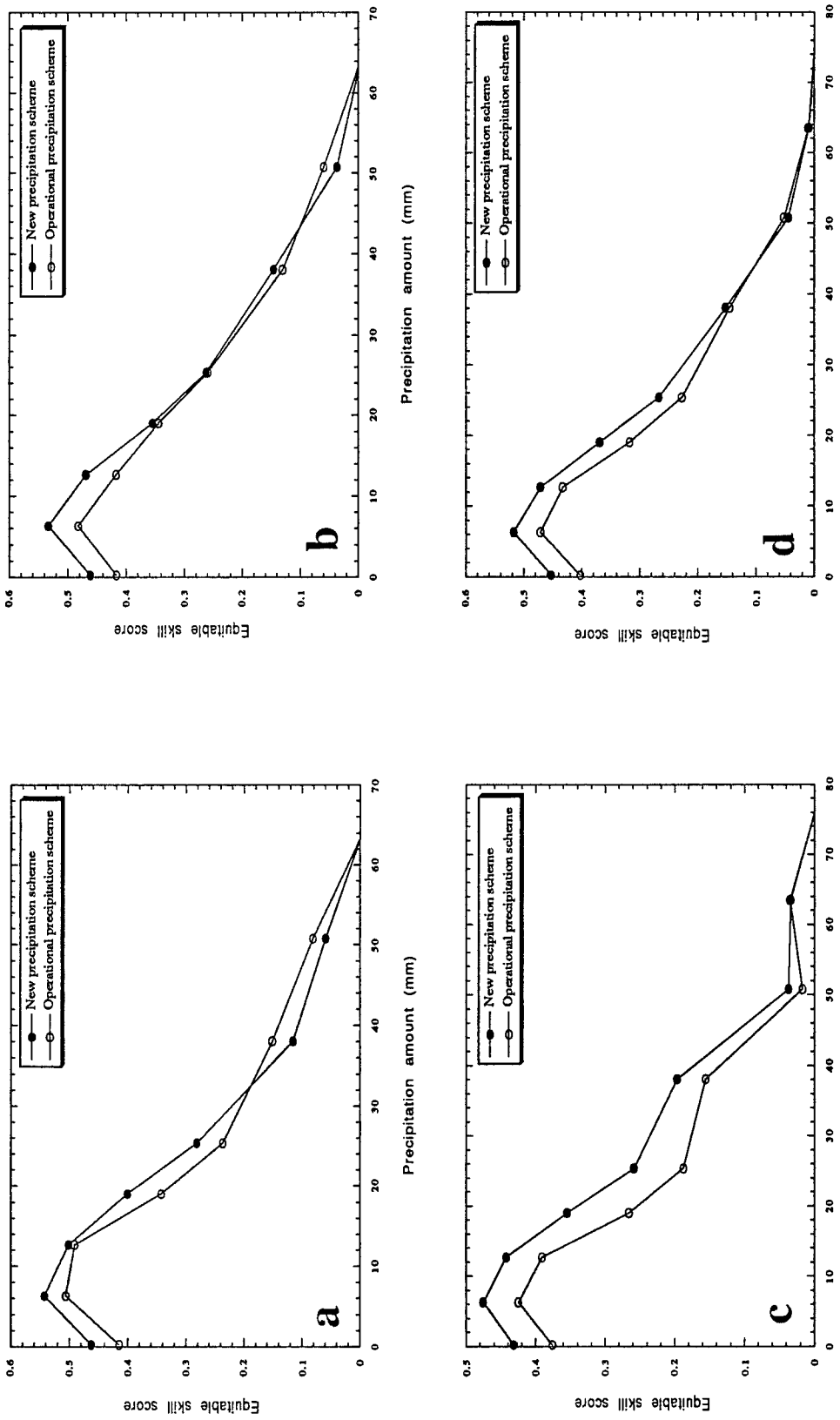

FIG. 9. Average equitable skill scores for precipitation forecasts from the operational and new precipitation schemes in test IV: (a) 0–24-h forecasts; (b) 12–36-h forecasts; (c) 24–48-h forecasts; (d) all forecasts.

TABLE 4. Description of the experiments in the Gilbert case study.

Experiment	Explanation
CONTROL	Eta Model with new precipitation scheme
OPERATIONAL	Operational Eta Model
NO CLOUD ICE	Same as control run, but with no cloud ice in both large-scale and convective precipitation parameterizations
NO ADVECTION	Same as control run, but with no horizontal advection of clouds
NO CLOUD IN CONV. PREC.	Same as control run, but the prognostic cloud is not incorporated into the convective precipitation parameterization

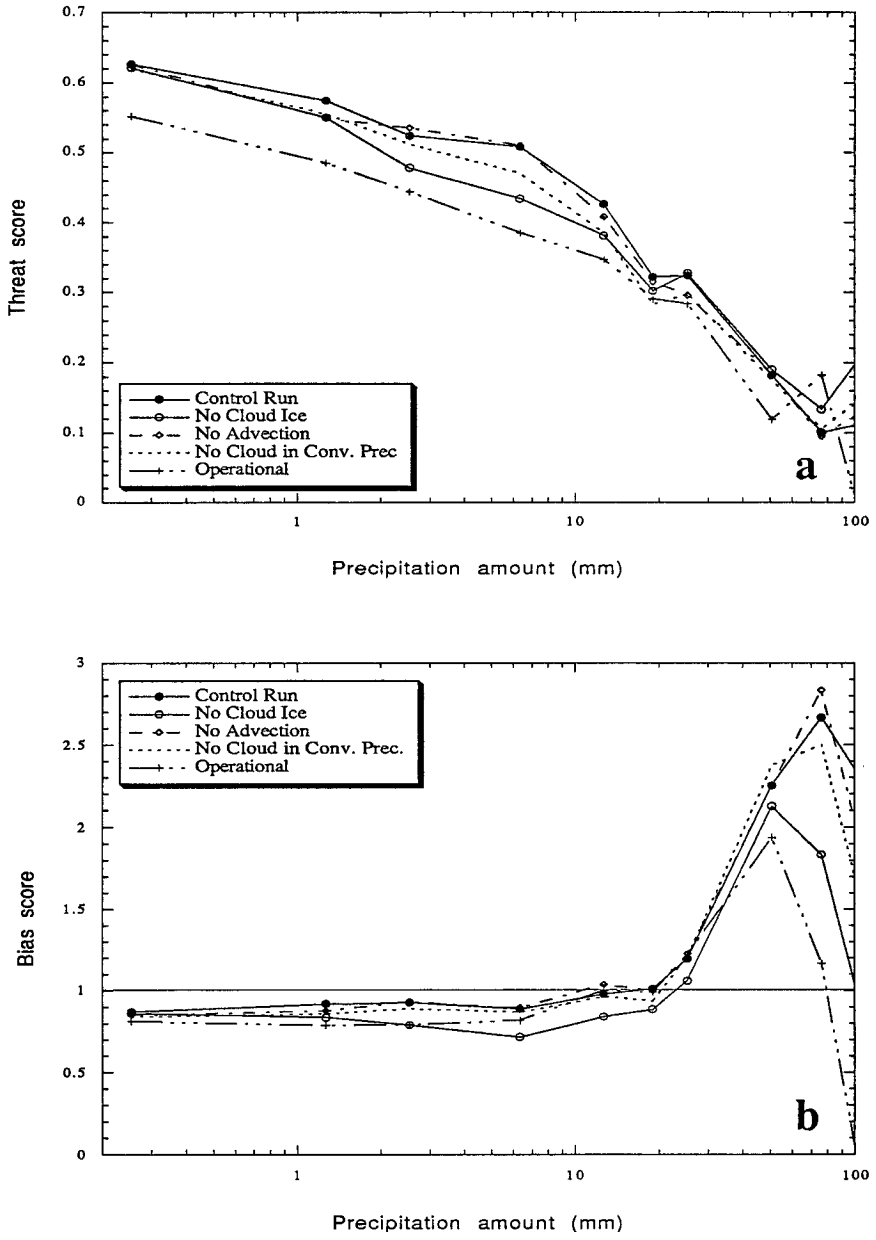

FIG. 10. The threat and bias scores of 24-h precipitation forecasts from the five experiments in the Gilbert case (18 September 1988) study.

to compare the results is to look at the average threat scores and biases of the 24- and 48-h precipitation forecasts from both models for each case. This was done by calculating the average threat scores and biases using the equations

$$\langle \text{THRT} \rangle_n = \sum_{i=1}^{M} b_{i,n} (\text{THRT})_{i,n} \tag{44}$$

$$\langle \text{BIAS} \rangle_n = \sum_{i=1}^{M} b_{i,n} (\text{BIAS})_{i,n}, \tag{45}$$

where M is the number of thresholds used in our threat and bias scores calculations, and the weight function $b_{i,n}$ was computed from

$$b_{i,n} = \frac{\begin{array}{c}\text{(grid number of observations}\\ \text{in each case for each threshold)}\end{array}}{\begin{array}{c}\text{(grid number of observations}\\ \text{in each case for all thresholds).}\end{array}} \tag{46}$$

Again this observation-weighted average eliminates the overweighting of scores from high precipitation amounts with just a few observation grid points. The calculated scores are presented in Fig. 6. The improvements in threat scores are again obvious. Compared with the operational results, only two 24-h forecasts and one 48-h forecast are slightly worse. There is no systematic change in the 24-h bias scores. The 48-h bias scores increased a little.

Table 3 indicates that test I was designed for winter- and springtime precipitation from stratiform clouds. The results shown in Figs. 5 and 6 indicate that the prognostic cloud scheme is successful in improving the stratiform, large-area precipitation forecasts. Two reasons are thought to be responsible for the improvements. First, the large-scale condensation represented by (8)–(11) is better than the operational scheme in that it relates the model large-scale condensation directly to the local changes of model temperature, pressure, and moisture fields. In other words, the precipitation field in the new model is more consistent with the synoptic situation than in the operational model where precipitation is calculated only from the moisture field. Second, cloud ice may play an important role in precipitation predictions, especially during winter and spring seasons. We will discuss this role after we show results from some individual experiments.

As an example of the precipitation forecasts from the cloud scheme, the precipitation pattern from a 24-h forecast of the experimental model on 13 April 1991 (case 20 in Fig. 6) is given in Fig. 7a, together with the operational forecast and the precipitation analysis given in Figs. 7b and 7c, respectively, for that time. The 20-mm contour in Fig. 7a is closer to the observed contour, although both forecasts underpredicted the heavy rainfall in southeast Arkansas. The new scheme also made a better forecast in Iowa. Another advantage of the precipitation scheme is its ability to predict precipitation type. As shown in Fig. 7a, circles indicate rain, while asterisks show the snow region. The crosses are regions where both snow and rain fell to the ground during the forecast period. To verify precipitation-type prediction, precipitation-type observations reported from about 50 stations located near the rain–snow boundaries are also plotted in Fig. 7c. Good agreement between the model prediction and the observed precipitation types is found in the northern and northwestern part of the precipitation region. In the northeastern part of the precipitation area, the model overpredicted the area of snow and mixed precipitation, especially in New York and northeastern Pennsylvania. However, snowfall was observed at Binghamton, New York.

Test IV is a parallel run made to test the cloud scheme for late spring and early summer precipitation forecasts. Both strong convection and large-scale stratiform precipitation were observed. This test was performed continuously in an operational mode from 14 April to 4 May 1992 and no case selections were made. Forecasts were carried out twice daily, starting at 0000 and 1200 UTC. To avoid the effects of changes in precipitation biases on the evaluation of precipitation forecast skill, equitable threat scores and equitable skill scores averaged for the parallel test period were calculated for all 0–24-, 12–36-, and 24–48-h precipitation forecasts from both the experimental model and the operational model (Figs. 8 and 9, respectively). The total scores for the whole period were also calculated. It should be noted that the equitable threat score is usually lower than other scores (by definition), and the changes in skill of precipitation forecasts are not as notable. Even so, the improvement in equitable threat scores at the 0.25-mm threshold for all three forecast periods is still obvious in Fig. 8. Figures 8 and 9 show that some improvements in precipitation forecasts have been made by the cloud scheme, particularly in the forecasts of light precipitation. If we look at the scores for heavy precipitation, however, we find that the results from the experimental model forecasts in this test are not as good as those in test I, especially in the 0–24-h forecasts. This problem was also found in test II, performed in August 1991 (not shown). This is probably caused by the strong convection present during these tests. Since the interactions between the microphysical processes and the Betts–Miller convective adjustment scheme in the experimental model are not well understood, more studies are needed for further investigation. Based on this consideration, the operational version of the prognostic cloud scheme does not combine the cloud physics with the Betts–Miller convective adjustment scheme.

To investigate the effect of clouds on precipitation forecasts, some special experiments were carried out for the period in which Hurricane Gilbert affected the United States in 1988. Gilbert made landfall at the northeast coast of Mexico on 17 September 1988 and then moved northeastward, producing a large area of heavy precipitation over Texas and Oklahoma. A more detailed description of this case can be found in a study by Baldwin

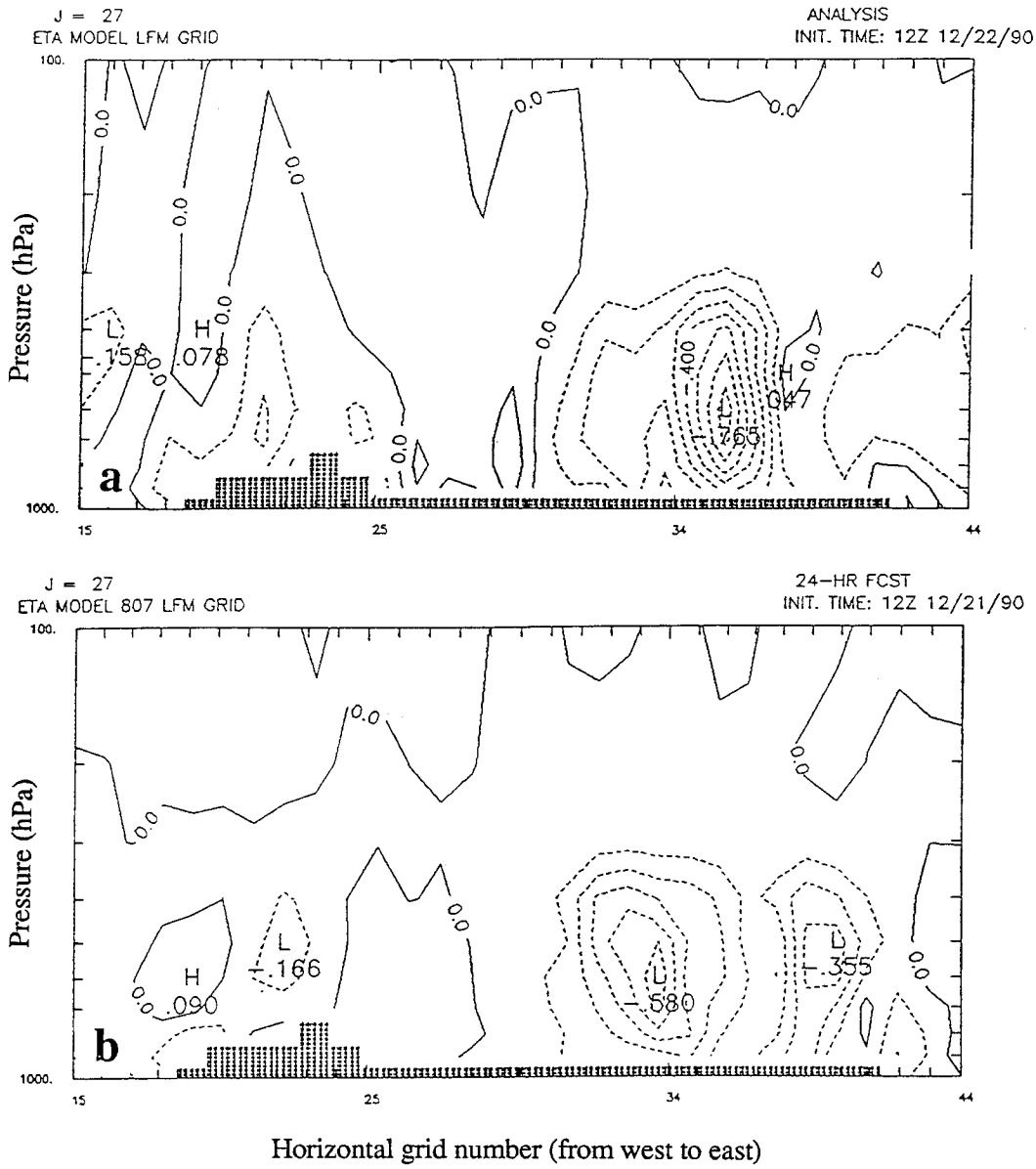

FIG. 11. Vertical cross sections of the vertical motion ω at 1200 UTC 22 December 1990. (a) Analysis; (b) 24-h forecast of the operational Eta Model; (c) 24-h forecast of the experimental Eta Model; (d) same as (c) except that cloud ice was not included. Contour interval is 0.1 Pa s^{-1}.

(1991). Table 4 gives the name and description of five experiments performed with this case. For each experiment, a 24-h forecast was made and the threat and bias scores were calculated using the hourly observations of precipitation obtained from Baldwin (1991) (Fig. 10). First it can be seen from Fig. 10a that the threat scores from the complete experimental model (CONTROL) are best, while the scores from the operational run (OPERATIONAL) are worse than the others for almost all precipitation categories. It is interesting to note that the threat scores from the run without cloud ice (NO CLOUD ICE) are significantly lower than those from the CONTROL, indicating the importance of cloud ice on precipitation even in this tropical storm case. It is well known that water vapor is more easily transformed to precipitation in regions where cloud ice exists than in regions without cloud ice, owing to the lower saturation vapor pressure over ice surfaces. This can be seen in Fig. 10b where the bias from the NO CLOUD ICE run is much lower than in the CONTROL, especially in the heavy precipitation range. This point will be discussed further in section 3c(3).

Another feature we can see in Fig. 10 is that the threat scores from NO CLOUD IN CONV. PREC. are lower than those from CONTROL for all thresholds, with the maximum difference between the 2.5- and 25-mm pre-

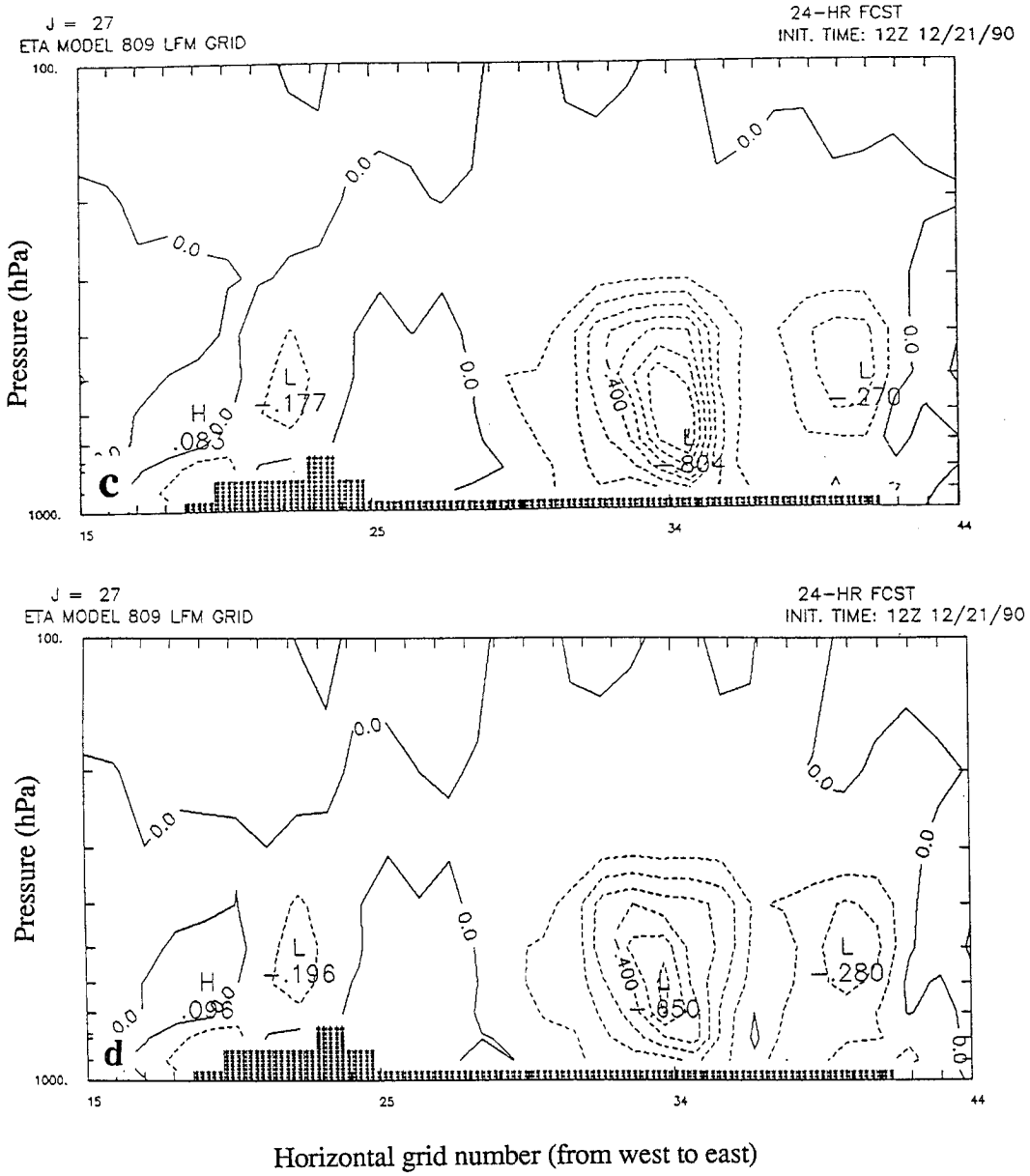

FIG. 11. (*Continued*)

cipitation amounts. It appears, at least from this case, that the introduction of cloud water/ice into the model's convective precipitation scheme can also improve the precipitation forecasts. More theoretical and experimental studies, however, are needed to get a clearer physical insight of the effects of clouds on modeled convection. Finally, the difference between the precipitation forecasts from the CONTROL and from the run without horizontal cloud advection (NO ADVECTION) seems to be insignificant, indicating that horizontal cloud advection has no obvious effect on precipitation forecasts. Note, however, that this experiment was carried out on an 80-km grid system. If we increase the model grid resolution, the results may be different.

The winter case of 21 December 1990 was selected to study the effects of cloud water/ice on large-scale precipitation forecasts. The new precipitation scheme improved the precipitation forecasts significantly in this case (not shown). The vertical cross section of vertical motion (ω) fields from the analysis and model 24-h forecasts along a line from Boston, Massachusetts, through Lake Superior to Seattle, Washington, is presented in Fig. 11. It is apparent that the upward motion in the main updraft region over the eastern part of the continent from the experimental model (Fig. 11c) has increased and agrees more with the analyzed values. Both operational and experimental model forecasts have some phase errors in the position of the updraft regions.

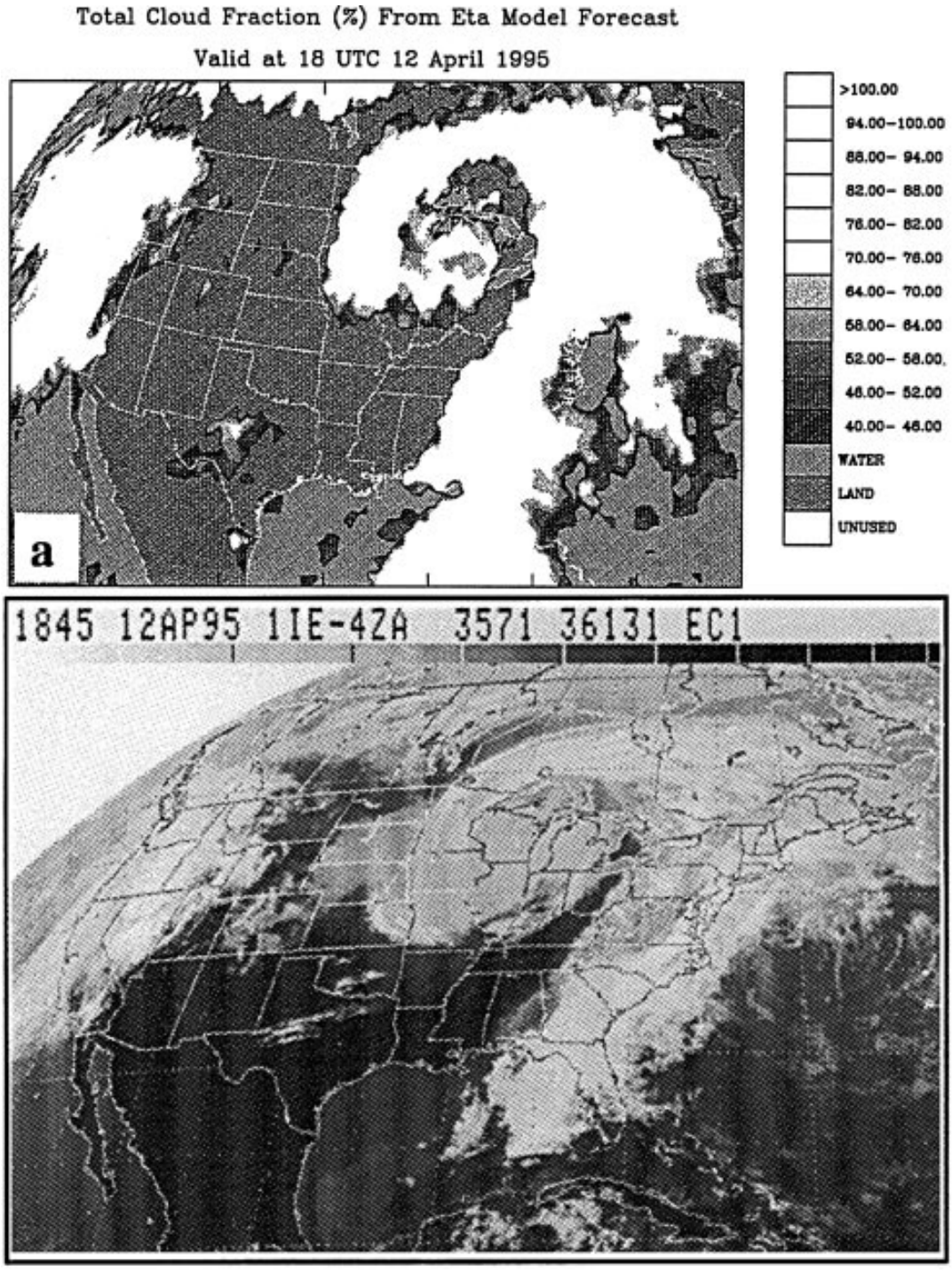

FIG. 12. (a) Total cloud fraction (percent) from an 18-h forecast of the experimental Eta Model valid at 1800 UTC 12 April 1995. (b) Infrared satellite image for 1845 UTC 12 April 1995.

It is also apparent, by comparing Figs. 11a–c, that the latent heating released from the microphysical processes appears to shift the maximum upward motion eastward toward the analyzed position.

2) CLOUD FORECASTS

In the prognostic cloud scheme, two cloud quantities are calculated. One is cloud coverage and the other is cloud water/ice mixing ratio. Ideally, an objective verification of cloud forecasts would be made quantitatively using the observed cloud data. However, there is no direct observation of three-dimensional cloud water/ice mixing ratio available. Hence, we will verify the horizontal distribution of clouds with the aid of satellite cloud pictures.

Figure 12a shows the total cloud fraction valid at 1800 UTC 12 April 1995 for an 18-h forecast from the experimental model. A well-defined comma-cloud pattern is associated with the prediction of a cyclonic storm over the eastern part of the United States. Figure 12b is the satellite picture about 45 min later. The consistency between Figs. 12a and 12b is quite high, especially at the rear edge of the cloud system.

Figures 13a, 13b, and 13c show the 24-h forecasts of the vertical cross sections of temperature, cloud water/ice mixing ratio, and the 12-h accumulated precipitation, respectively, valid at 1200 UTC 22 December 1990 along the cross section in Fig. 11. A large cloud system over the eastern part of the continent is clearly represented in Fig. 13b. The structure of the cloud system is consistent with a mature midlatitude cyclone (see, e.g., Carlson 1980). The cloud water/ice mixing ratio maximum near *A* is associated with precipitation produced by the ''warm conveyer belt'' as air is lifted ahead of the low pressure center. The relative minimum between *A* and *B* is due to the dry tongue of the mature cyclone. The maximum near *B* is the ''comma head'' region where the cold conveyer belt and midlevel vorticity advection produce rising motion at lower elevations. We also observe and forecast a small amount of orographic precipitation just west of the Continental Divide. Hence Fig. 13b shows a primarily nonprecipitating cloud produced by the cloud scheme. Nonprecipitating clouds may not be important to model precipitation forecasts but may be important to model radiation calculations.

A time–height cross section of clouds and the associated precipitation rate at a point located in the center of the large precipitation area near Memphis, Tennessee, produced from the experimental model 48-h forecast starting at 1200 UTC 21 December 1990 is presented in Fig. 14. More than 20 mm of precipitation was predicted at this point during the first 24 h. It is clear that there are basically two cloud layers during the first 15 h at this point. The model temperatures (not shown) show that the freezing level at that time was located between levels 7 and 8, indicating that the upper cloud layer consists mainly of ice particles, while the lower cloud layer is mainly liquid water drops. The seeding effects of the liquid water clouds by the ice particles (snow precipitation in this scheme) from the ice clouds above is reflected by the strong precipitation between 8 and 13 h shown in Fig. 14b. After 24 h, a surface cold front passed by this point and precipitation ended. Only a few low-level clouds and some cirrus were found after the cold-frontal passage.

3) CLOUD ICE EFFECTS

To study the impact of the inclusion of ice-phased clouds in the cloud scheme on precipitation and cloud water content, a special experiment was conducted with cloud ice excluded for the same case, as shown in Figs. 11 and 13. A cross section of vertical motion ω is given in Fig. 11d, while cross sections of temperature and cloud water mixing ratio are shown in Figs. 15a and 15b, respectively. The corresponding 12-h accumulated precipitation is given in Fig. 15c.

It should be pointed out that most clouds in Fig. 13b consist of ice particles because of the cold temperature shown in Fig. 13a, while the clouds in Fig. 15b are constrained to consist of liquid water only. There is no notable difference between Figs. 13a and 15a, indicating that the extra latent heating released by the inclusion of ice-phased clouds is relatively small compared to other large-scale forcing. However, a large difference between the ω fields shown in Figs. 11c and 11d is found in the main updraft regions. Thus, the small increases in latent heating by the inclusion of cloud ice, especially at low levels, causes significant increases in vertical motion.

It is interesting to notice, by comparing Fig. 15 with Fig. 13, that the inclusion of cloud ice increases cloud water/ice content in nonprecipitating clouds but decreases cloud water/ice content in precipitating clouds. It is known that water vapor deposits more easily on ice particles than on water droplets, producing more cloud water/ice content in regions where ice particles exist. Once precipitation starts, however, cloud water/ice is effectively removed with precipitation. The stronger the precipitation is, the more cloud water/ice is removed. It is seen from Figs. 13c and 15c that precipitation is increased by the inclusion of cloud ice, and, as a result, more cloud water/ice is removed from the clouds above by the stronger precipitation in that area.

4. Summary and discussion

A prognostic cloud parameterization scheme in which cloud water and cloud ice, as well as some microphysical processes for precipitation production, are included is proposed and extensively tested. Significant improvements in precipitation forecasts are successfully demonstrated using the Eta Model at NCEP. The cloud fields predicted from this scheme are consistent with satellite cloud imagery and typical synoptic-scale structure. Precipitation types can also be predicted by this scheme and are basically consistent with observations.

A few comments will be made here to provide a better

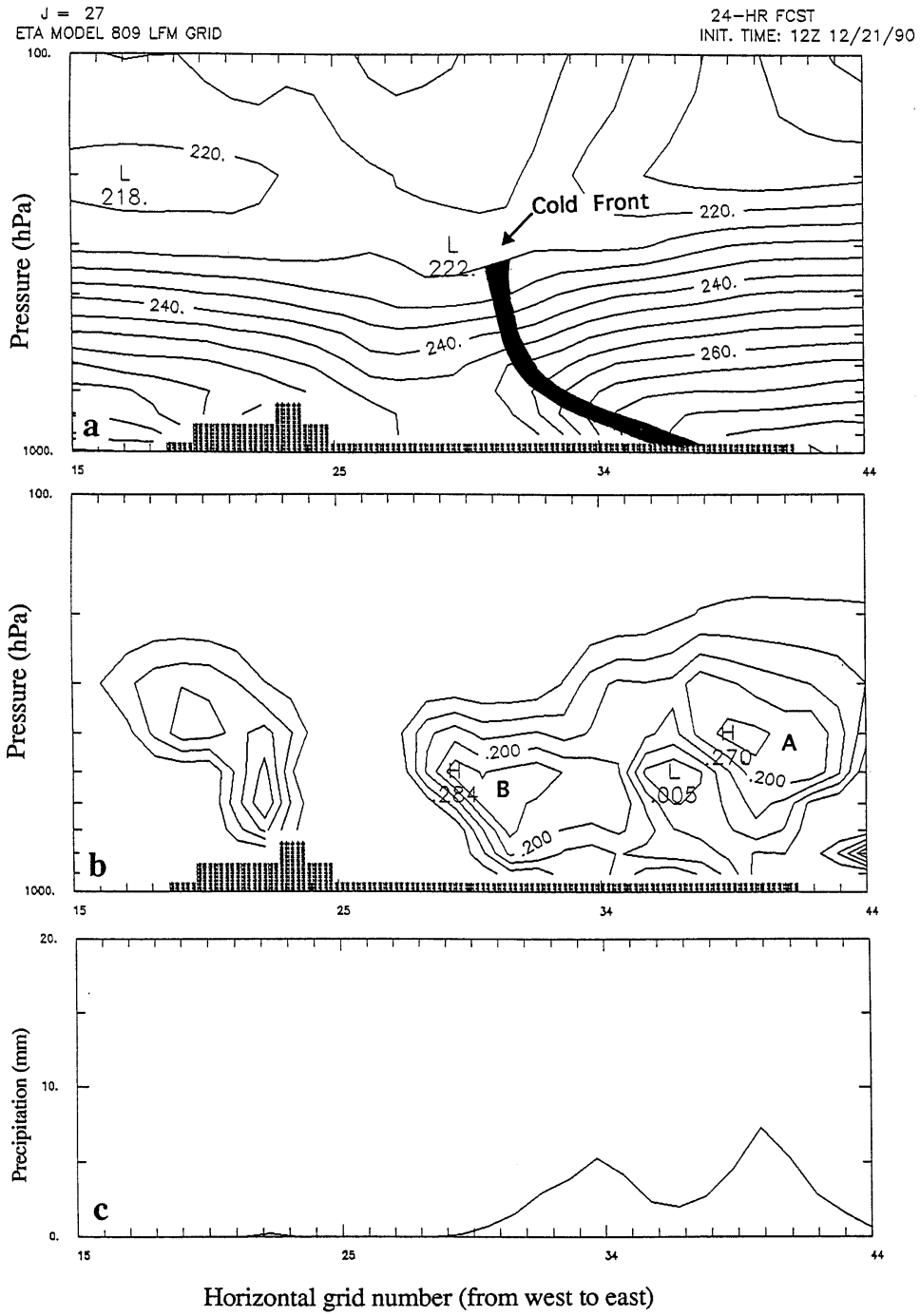

FIG. 13. Vertical cross sections of (a) temperature (K), (b) cloud water/ice mixing ratio, and (c) 12-h accumulated precipitation (mm) along the cross section shown in Fig. 11 at 1200 UTC 22 December 1990 from the 24-h forecast by the experimental Eta Model. Contour interval in (b) is 0.05 g kg^{-1}.

understanding of how the new scheme improves model forecasts, especially precipitation forecasts, over the old scheme. First, the new precipitation scheme is better than the old one in that the introduction of clouds makes the model's hydrological cycle more complete. Second, unlike the old scheme that calculates condensation and precipitation as one process, the new scheme separates these two physical processes. All condensed water goes into clouds and then precipitation is produced from clouds when condensed water/ice becomes sufficient.

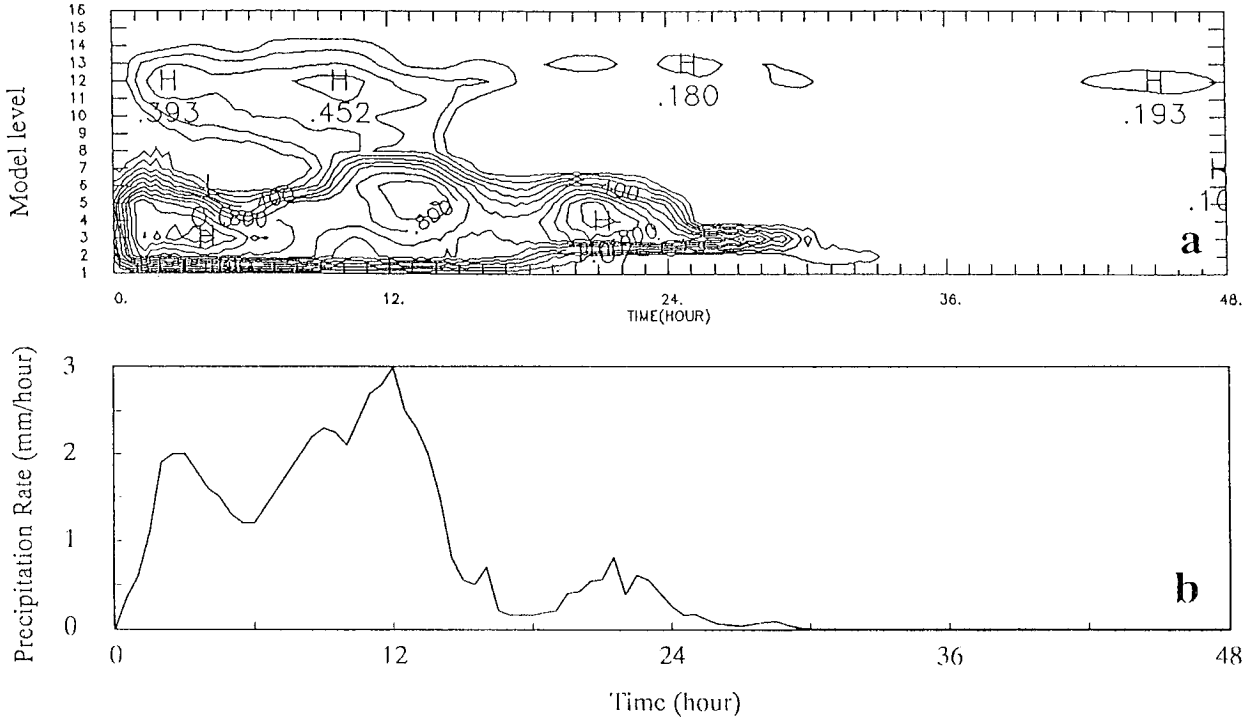

FIG. 14. (a) Time–height section of cloud water/ice mixing ratio at a point near the center of heavy precipitation for the case of 22 December 1990 (contour interval is 0.1 g kg^{-1}). (b) The corresponding precipitation rate (mm h^{-1}).

This allows only part of the condensed water/ice to fall as precipitation and the rest to stay in the atmosphere as nonprecipitating clouds and move with the air. Third, the large-scale condensation method used in the new scheme calculates condensation based on not only relative humidity, but also changes of temperature, moisture, and pressure. In other words, it is more thermodynamically and hydrologically consistent with the model. Furthermore, the inclusion of ice-phased clouds in the new scheme makes calculations of condensation/deposition and precipitation, as well as latent heating release, more realistic.

The statistical results and case studies previously discussed provide very useful information on how an NWP model performs with the inclusion of cloud water/ice, as well as additional physical insight and understanding of the explicit description of cloud water/ice in NWP models, an area in which our knowledge is limited. Large differences between versions were found in precipitation and vertical motion fields. As discussed earlier, the realistic description of clouds and the associated microphysical processes in the new scheme produce more accurate location and amounts of precipitation. However, improved vertical motion is obviously another important factor for the changes in precipitation forecasts. The new scheme cannot only enhance upward motion in strong condensation regions but also reduce it in regions where the upward motion from the old scheme is stronger than observed. These features can easily be found in Fig. 11. Horizontal shifts of the vertical motion field by the new scheme were also found on 700-hPa ω maps (not shown). Apparently, the inclusion of cloud ice is proved to be important in the vertical motion changes.

It is found that changes in the wind field by the inclusion of explicit clouds are not significant. Thus, the feedback to dynamical fields from cloud microphysics is secondary compared to other major processes (e.g., advection). But this result may be strongly dependent on model resolution.

There are currently no routine, direct observations of the three-dimensional cloud water/ice mixing ratio. The cloud water and cloud ice are currently set to zero everywhere at the initial time of model integration. Thus, our experimental Eta model suffers from, in addition to an inadequate initial cloud field, an inconsistent specification of the moisture field. To address this problem, a method is needed to incorporate observed precipitation and cloud data into the Eta Model data assimilation system to initialize the model moisture, cloud, and latent heating. A cloud initialization scheme for the Eta Model was proposed by Zhao (1993) and will be tested and implemented at NCEP in the near future.

Acknowledgments. The authors wish to express our deep appreciation to Dr. Glen Lesins for his many helpful hours of guidance and suggestions to this research.

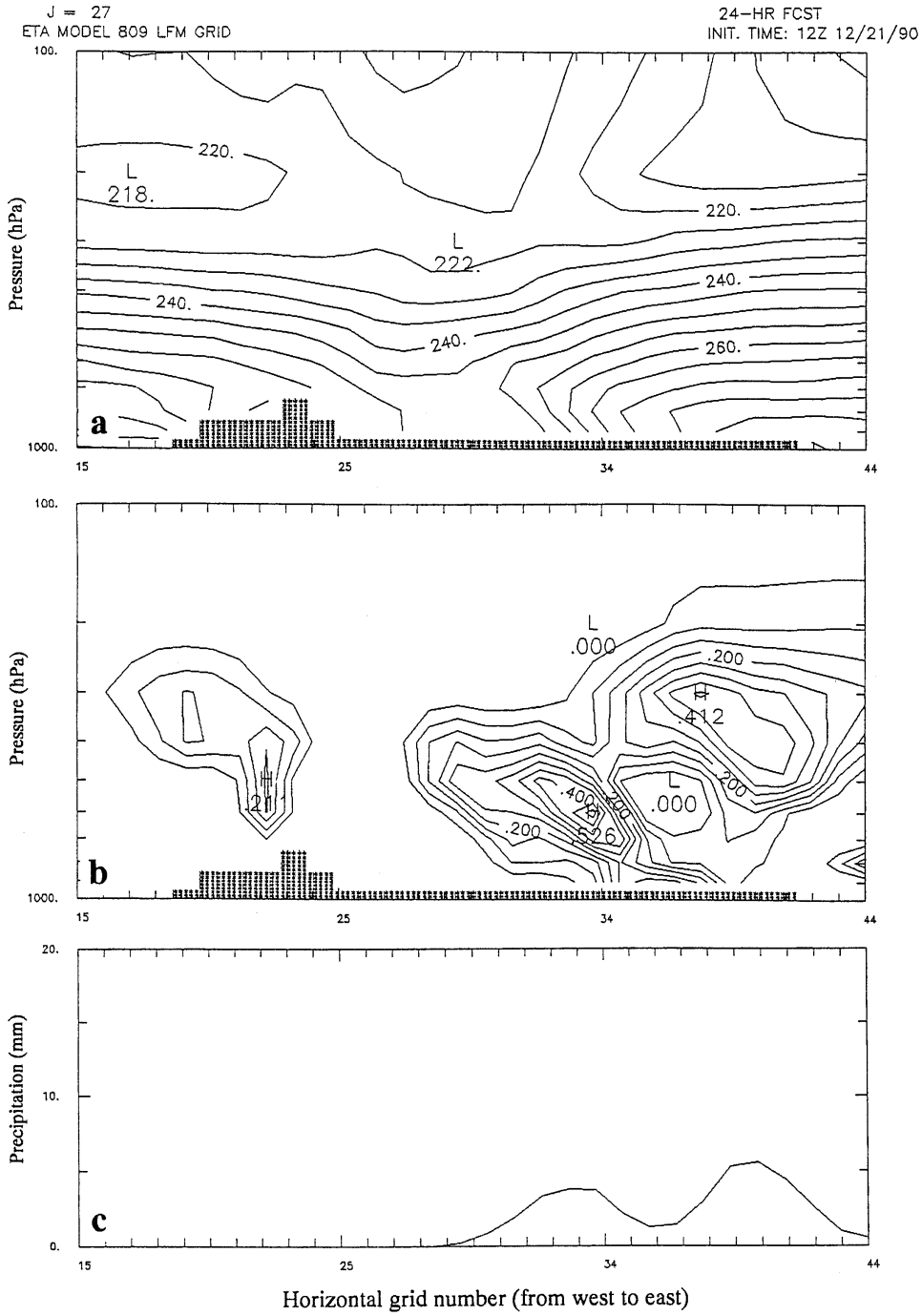

FIG. 15. Same as Fig. 13 except that ice-phase cloud is not included in microphysics.

Thanks also go to Drs. Eugenia Kalnay and Geoff DiMego for their leadership and continuous support of this work. The authors are very grateful to Drs. Thomas Black, Fedor Mesinger, Kenneth Mitchell, Eric Rogers, and Joseph Gerrity for their encouragement and suggestions. Special thanks go to Mr. Michael Baldwin for his help over the past several years. This research is a contribution from the National Science Foundation/National Meteorological Center Joint Program on Numerical Weather Prediction and was supported by NSF Grant ATM-8807752. The Center for Analysis and Prediction of Storms at the University of Oklahoma (NSF Grant ATM91-20009) is acknowledged for their support of the completion of this work.

APPENDIX

Definition of Objective Verification Scores for Precipitation

For objective evaluation of quantitative precipitation forecasts, four scores were calculated in this study. Bias (BIAS) and threat (THRT) scores are given by

$$\text{BIAS} = \frac{F}{O} \tag{A1}$$

$$\text{THRT} = \frac{H}{O + F - H}, \tag{A2}$$

where F is the number of forecast points above a threshold, O is the number of observed points above a threshold, and H is the number of hits (i.e., correct forecasts) above a threshold. Equitable threat score (EQTS) is defined as

$$\text{EQTS} = \frac{H - \text{CH}}{F + O - H - \text{CH}}, \tag{A3}$$

where CH is the expected number of hits in a random forecast of F points for O observed points, which is equal to

$$\text{CH} = \frac{FO}{M}, \tag{A4}$$

where M is the number of points to be verified. Equitable skill score (EQSS) is computed using the equation

$$\text{EQSS} = W_{11}P_{11} + W_{12}P_{12} + W_{21}P_{21} + W_{22}P_{22}, \tag{A5}$$

where

$$P_{11} = \frac{H}{M} \qquad W_{11} = \frac{M - O}{O}$$

$$P_{12} = \frac{O - H}{M} \qquad W_{12} = -1$$

$$P_{21} = \frac{F - H}{M} \qquad W_{21} = -1$$

$$P_{22} = \frac{M - O - F + H}{M} \qquad W_{22} = \frac{O}{M - O}.$$

REFERENCES

Baldwin, M. E., 1991: Incorporation of precipitation data into a numerical weather prediction data assimilation system. M.S. thesis, School of Meteorology, University of Oklahoma, 143 pp. [Available from the School of Meteorology, University of Oklahoma, 100 E. Boyd St., EC Room 1310, Norman, OK 73019.]

Betts, A. K., 1986: A new convective adjustment scheme. Part I: Observational and theoretical basis. *Quart. J. Roy. Meteor. Soc.*, **112,** 677–691.

——, and M. J. Miller, 1986: A new convective adjustment scheme. Part II: Single column tests using GATE wave, BOMEX, ATEX and Arctic air-mass data sets. *Quart. J. Roy. Meteor. Soc.*, **112,** 693–709.

Black, T. L., 1994: The new NMC mesoscale Eta Model: Description and forecast examples. *Wea. Forecasting,* **9,** 265–278.

——, and F. Mesinger, 1989: Forecast performance of NMC's eta coordinate regional model. Preprints, *12th Conf. on Weather Analysis and Forecasting,* Monterey, CA, Amer. Meteor. Soc., 551–555.

——, Z. I. Janjić, and J. H. Ward, 1990: Heavy precipitation forecasts from NMC's eta model. Preprints, *16th Conf. on Severe Local Storms,* Kananaskis Park, AB, Canada, Amer. Meteor. Soc., J1–J4.

Carlson, T. N., 1980: Airflow through midlatitude cyclones and the comma cloud pattern. *Mon. Wea. Rev.*, **108,** 1498–1509.

Fels, S. B., and M. D. Schwarzkopf, 1975: The simplified exchange approximation: A new method for radiative transfer calculations. *J. Atmos. Sci.*, **32,** 1475–1488.

Golding, B. W., 1990: The Meteorological Office mesoscale model. *Meteor. Mag.*, **119,** 81–96.

Hoke, J. E., N. A. Phillips, G. J. DiMego, J. J. Tuccillo, and J. G. Sela, 1989: The regional analysis and forecast system of the National Meteorological Center. *Wea. Forecasting,* **4,** 323–334.

Janjić, Z. I., 1984: Nonlinear advection schemes and energy cascade on semistaggered grids. *Mon. Wea. Rev.*, **112,** 1234–1245.

——, 1990: The step-mountain coordinate: Physical package. *Mon. Wea. Rev.*, **118,** 1429–1443.

——, 1994: The step-mountain eta coordinate model: Further developments of the convection, viscous sublayer, and the turbulence closure scheme. *Mon. Wea. Rev.*, **122,** 927–945.

Kessler, E., 1969: *On the Distribution and Continuity of Water Substance in Atmospheric Circulations. Meteor. Monogr.,* No. 32, Amer. Meteor. Soc., 84 pp.

Lacis, A. A., and J. E. Hansen, 1974: A parameterization of the absorption of solar radiation in the earth's atmosphere. *J. Atmos. Sci.*, **31,** 118–133.

Lin, Y.-L., R. D. Farley, and H. D. Orville, 1983: Bulk parameterization of the snow field in a cloud model. *J. Climate Appl. Meteor.*, **22,** 1065–1092.

Mellor, G. L., and T. Yamada, 1974: A hierarchy of turbulence closure models for planetary boundary layers. *J. Atmos. Sci.*, **31,** 1791–1806.

——, and ——, 1982: Development of a turbulence closure model for geophysical fluid problems. *Rev. Geophys. Space Phys.*, **20,** 851–875.

Mesinger, F., Z. I. Janjić, S. Nicković, D. Garilov, and D. G. Deaven, 1988: The step-mountain coordinate: Model description and performance for cases of Alpine lee cyclogensis and for a case of an Appalachian redevelopment. *Mon. Wea. Rev.*, **116,** 1493–1518.

Pudykiewicz, J., R. Benoit, and J. Mailhot, 1992: Inclusion and verification of a predictive cloud-water scheme in a regional numerical weather prediction model. *Mon. Wea. Rev.*, **120,** 612–626.

Rogers, R. R., 1979: *A Short Course in Cloud Physics.* 2d ed. Pergamon Press, 130 pp.

Rutledge, S. A., and P. V. Hobbs, 1983: The mesoscale and microscale structure and organization of clouds and precipitation in midlatitude cyclones. VIII: A model for the ''seeder-feeder'' process in warm-frontal rainbands. *J. Atmos. Sci.*, **40,** 1185–1206.

Smith, R. N. B., 1990: A scheme for predicting layer clouds and their water contents in a general circulation model. *Quart. J. Roy. Meteor. Soc.*, **116,** 435–460.

Sundqvist, H., 1978: A parameterization scheme for non-convective condensation including prediction of cloud water content. *Quart. J. Roy. Meteor. Soc.*, **104,** 677–690.

——, 1988: Parameterization of condensation and associated clouds in models for weather prediction and general circulation simulation. *Physically-Based Modelling and Simulation of Climate and Climatic Change, Part I,* M. E. Schlesinger, Ed., Reidel, 433–461.

——, E. Berge, and J. E. Kristjánsson, 1989: Condensation and cloud studies with a mesoscale numerical weather prediction model. *Mon. Wea. Rev.*, **117,** 1641–1657.

Tiedtke, M., 1993: Representation of clouds in large-scale models. *Mon. Wea. Rev.*, **121,** 3040–3061.

Zhao, Q., 1993: The incorporation and initialization of cloud water/ice in an operational forecast model. Ph.D. dissertation, University of Oklahoma, 195 pp. [Available from the School of Meteorology, University of Oklahoma, 100 E. Boyd St., EC Room 1310, Norman, OK 73019.]